2015

Accurate modelling and positioning of a magnetically-controlled catheter tip

Vi T. H. Le
Edith Cowan University

Edith Cowan University

Copyright Warning

USE OF THESIS

The Use of Thesis statement is not included in this version of the thesis.

EDITH COWAN UNIVERSITY

ACCURATE MODELLING AND POSITIONING OF A MAGNETICALLY-CONTROLLED CATHETER TIP

By

VI THANH NGUYEN LE

This thesis is presented in fulfilment of the requirements for the degree of Master of Computer Science

SCHOOL OF COMPUTER & SECURITY SCIENCE
FACULTY OF, HEALTH, ENGINEERING AND SCIENCE
EDITH COWAN UNIVERSITY

06/2015

ABSTRACT

This thesis represents the initial phase of a proposed operator and patient friendly method designed to semi-automate the positioning and directing of an intravascular catheter in the human heart using a variable electromagnetically induced field to control a catheter tip equipped with three tiny fixed magnets oriented in XYZ planes. Here we demonstrate a comprehensive mathematical model which accurately calculates the magnetic field generated by the electromagnet system, and the magnetic torques and forces exerted on a three-magnet tip catheter. From this we have developed an iterative predictive computer algorithm to show the displacement and deflection of the catheter tip. Using an eight variable power electromagnet system around a 250mm sphere of air we have proven the ability of this to accurately move the catheter tip from an initial position to a designated position within the field.

DECLARATION

I certify that this thesis does not, to the best of my knowledge and belief:

(i) incorporate without acknowledgement any material previously submitted for a degree or diploma in any institution of higher education;

(ii) contain any material previously published or written by another person except where due reference is made in the text; or

(iii) contain any defamatory material.

I also grant permission for the Library at Edith Cowan University to make duplicate copies of my thesis as required.

Vi Thanh Nguyen Le

ACKNOWLEDGEMENTS

The author would like to sincerely thank the following individuals: Firstly, I would like to thank Professor Kamal Alameh. His guidance, mentorship, and not to mention the many hours of time committed to proof-reading draft manuscripts proved to be invaluable to my educational experience. Secondly, my academic advisor, Dr. Nghia Hoang, whose support and advice greatly facilitated this project. His wide knowledge has taught me many valuable lessons and helped me to complete this work. He has provided me with a massive source of information throughout my journey. I would like to thank you both from the bottom of my heart. Finally, I express my deep gratitude to my parents for being there until the end and giving me all the support I need to finish this thesis.

TABLE OF CONTENTS

LIST OF FIGURES

LIST OF TABLES

LIST OF ABBREVIATIONS

AF	Atrial Fibrillation
BVP	Boundary Value Problem
CGCI	Catheter Guidance, Control and Imaging system
DC	Direct Current
DOF	Degree Of Freedom
FEM	Finite Element Method
IVP	Initial Value Problem
MDT	Magnetic Deflection Tester
MGS	Telstar Magnetic Guidance System
NdFeB	Neodymium-iron-boron
ODE	Ordinary Differential Equation
RF	Radio Frequency

NOMENCLATURE

[C1…C8]	Ordinal number of eight electromagnets
d_{inner}	Inner diameter
d_{outer}	Outer diameter
d_{core}	Core diameter
L_{coil}	Length of coil
L_{core}	Length of core

Calculating the total magnetic field of coils

$P(x_P, y_P, z_P)$	A point in the central 3D workspace
dl	Arc length of a current element
L	Length of each divided current element
Nl	Number of layers
Nt	Number of turns
Ns	Number of segments
n^{th}	Ordinal number of coil
i	Increment for the number of layers
j	Increment for the number of turns
k	Increment for the number of current elements
$\vec{B}_{Coil\,n}$	The total magnetic field of coil n^{th}

Calculating the total magnetic field of iron cores

$\vec{M}$	Magnetization vector of the iron core at the magnetic dipole
dV	Volume of a small magnetic dipole element
$d\vec{m}$	Magnetic moment of a small magnetic dipole element
dr	Spacing between turns
dz	The mesh sizes along the horizontal direction
$d\theta$	Angular direction
$\vec{m}_c$	Unitary magnetic moment vector of iron core element
$\vec{B}_{core}(\vec{m}, \vec{P})$	The total magnetic field of core
μ_0	Vacuum magnetic susceptibility

$\vec{P}_{ijk}$	Distance vector from the iron core elements to the point P
dV_{ijk}	Volume of core elements

Homogenous transformation matrices

L^O	Matrices of a set of vectors that represent the global coordinates of the electric current elements and core elements according to the translation and rotation transformations
R_{Cn}^O	Rotation transformation from the local coordinate system of eight electromagnets relative to the global coordinate system Oxyz
T_{Cn}^O	Translation transformation from the local coordinate system of eight electromagnets relative to the global coordinate system Oxyz
L^{Cn}	Matrices of a set of vectors that represent the local coordinates of the electric current elements and core elements in the Cn^{th} electromagnet, where each column of these matrices consists of the components of the corresponding vector of the set

Calculating torques and forces

M_{12}	Bending moment between the first magnet and second magnet
M_{23}	Bending moment between the second magnet and third magnet
M_{13}	Bending moment between the first magnet and third magnet
$\Delta\varphi_{N12}$	Bending moment M_{12} depends on the variable angle $\Delta\varphi_{N12}$
$\Delta\varphi_{N13}$	Bending moment M_{13} depends on the variable angle $\Delta\varphi_{N13}$
$\Delta\varphi_{N23}$	Bending moment M_{23} depends on the variable angle $\Delta\varphi_{N23}$
l_{12}	Spacing between the first magnet and second magnet

l_{13}	Spacing between the first magnet and third magnet
l_{23}	Spacing between the second magnet and third magnet
$\{F_{t1}, F_{t2}, F_{t3}\}$	Total forces exerted on three magnets
$\{F_{t1x},\ F_{t2x},\ F_{t3x}\}$	Total forces along the x-axis
$\{F_{t1y}, F_{t2y},\ F_{t3y}\}$	Total forces along the y-axis
$\{F_{m1}, F_{m2}, F_{m3}\}$	Magnetic forces on three magnets
$\{P_1, P_2, P_3\}$	Gravitational forces on three magnets
$\{\delta_{x1}, \delta_{x2}, \delta_{x3}\}$	Horizontal displacements
$\{\delta_{y1}, \delta_{y2}, \delta_{y3}\}$	Vertical displacements
$\{\varphi_{N1}, \varphi_{N2}, \varphi_{N3}\}$	Angles between the tangent to the curve (of each magnetic seed) and the x-axis
$\frac{d\varphi}{ds}$	The curvature of the catheter at any point along its length
EI	Bending rigidity of the catheter
$\{T_1, T_2, T_3\}$	The total of magnetic torques produced by the external magnetic field and the bending moments M_{12}, M_{23}, M_{13} among three magnets
M_0	A moment applied at the end of the tip is the total of magnetic torques
$\{M_1, M_2, M_3\}$	Bending moments at the three seed magnets of the catheter
{Ai, Bi}	Points at the front end of the i^{th} magnetic seed
ds	Arc length of the catheter
s	A variable runs from s = 0 at the fixed point of the catheter to s = L at the free end of the catheter

CHAPTER 1 INTRODUCTION

1.1 Motivation

Cardiovascular disease is one of the leading causes of mortality in the world. Half of the cardiovascular mortality is due to heart failure, i.e. progressive alteration of cardiac contraction. Cardiac contraction is entirely dependent on prior electrical activation, and therefore, a substantial number of cases of heart failure are secondary to or aggravated by electrical dysfunctions (ventricular dys-synchrony in more than 50%, atrial fibrillation in approximately 24%). Atrial Fibrillation (AF) in particular, diminishes the ability for the heart to function as a twin 2 stage pump to the body, thus reducing the fitness and capacity of the affected individual to perform daily routine duties and work. It also substantially increases the incidence of stroke, heart failure and overall mortality [1-3].

AF typically develops with increasing age: Approximately 5-10% of the population older than 60 years have this condition. Medical treatment (cardiac drugs) can diminish symptoms but does not permanently prevent the recurrence of arrhythmia. AF is a rapidly growing social, medical and public health problem requiring a significant effort in experimental, translational and clinical research to obtain better preventive and curative therapies and reduce the disease burden. As less than 5% of eligible patients can be currently treated by interventional ablation techniques, the number of clinical catheter laboratories dedicated to cardiac electrical disturbances is expected to be multiplied by 5 times in the next 10 years [3].

One of the effective minimally-invasive AF treatments is based on the use of a Radio Frequency (RF) catheter that ablates specific areas of the atrial myocardium in order to electrically isolate the four pulmonary veins in the left atrium [4, 5]. RF-based AF ablation procedures are significantly more effective than antiarrhythmic drugs and are performed with the aim of improving patient quality of life and reducing healthcare resource utilisation in the longer term [6-8]. Also, AF procedures help to enhance the effectiveness of standard therapeutics and ease the symptom burden for patients [9]. However, a major time consuming technical difficulty in RF catheter procedures is to accurately manipulate the tip of the catheter into its desired position and hold it there. This requires significant training and operator dexterity which is

highly variable in clinical practice. Rapid and accurate catheter tip positioning would much improve the procedure with potential benefits in safety and efficacy as well rendering the procedure more globally applicable and predictable. Remote magnetic catheter navigation is probably also applicable to similar intraluminal procedures in other fields of medicine such as interventional radiology and vascular surgery.

Technically, AF occurs in the atria, in the upper chambers of the heart and many impulses begin and spread chaotically through the atria. The result is that a person's heart beats is usually fast and irregular. The atria are said to be fibrillating when they beat too quickly and irregularly, during this time, they are unable to completely empty all of the blood they receive into the ventricles below, which can cause blood clots. These blood clots can then move to carotid arteries and block blood flow to the brain, causing a stroke as illustrated in Fig. 1.1 [4].

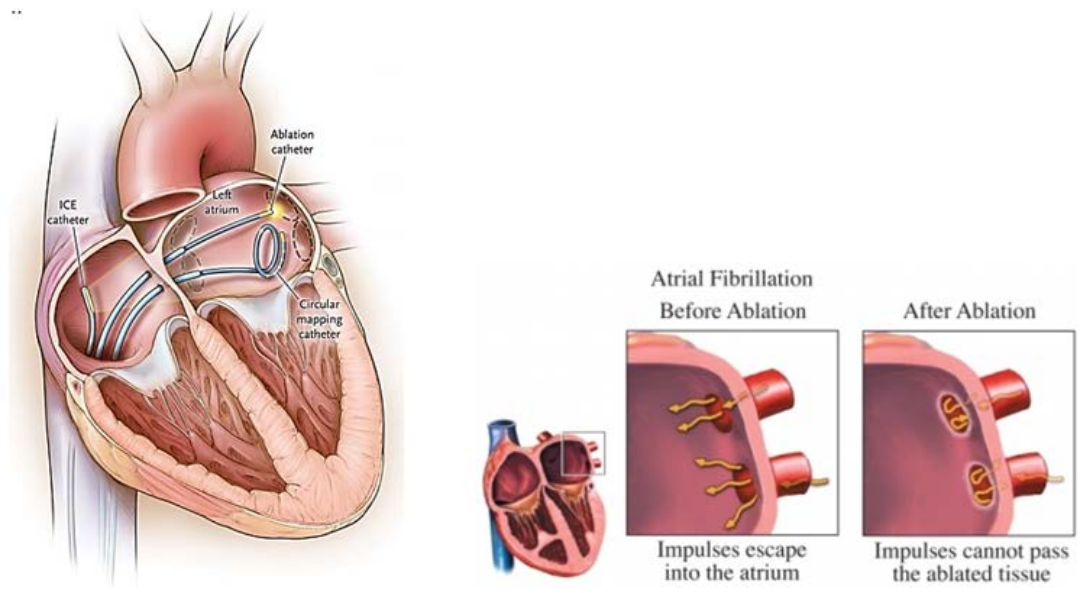

Fig. 1.1. An ablation catheter is inserted into the left atrium of the heart with respect to the mapping catheter to treat AF and the difference of the AF process between before ablation and after ablation [4].

The CGCI system, developed by Magnetecs Inc., has mainly been devised to overcome the shortcomings of the Niobe system. It comprises eight powerful coil-core electromagnets that can be placed around the torso to generate a high magnetic field (up to 0.14T) [10]. Due to the spherical arrangement of its eight electromagnets, the CGCI system dynamically creates an isotropic magnetic field and gradient

distribution along arbitrary directions, enabling faster motion of the catheter tip in real-time, and making it more stable [11-14]. While a mathematical model for positioning the catheter in the CGCI system has been reported in Refs [10, 13, 15], this mathematical model is limited to single-magnet-tip catheters. A three-magnet-tip catheter is able to displace more flexibly and have a large bending angle to reach expected positions within the heart. Therefore, this thesis develops a comprehensive mathematical model that accurately predicts the position of the three-magnet-tip catheter controlled by an externally applied magnetic field generated by an eight-electromagnet system.

1.2 Background to the study

The magnetic interactions have always inspired and motivated researchers, and as a result, there have been a myriad of findings about magnetic guidance in medical fields [16]. In the eighteenth century, the use of magnets for removing iron or steel splinters or objects from the interior of the eye and from other body parts was done successfully. This can be taken as an example to illustrate the use of magnetic interactions between two magnetized objects [16]. An important proof-of-concept demonstration was carried out in the 1950's by Tillander, who used, for the first time, a large external magnet to magnetically guide a transvascular catheter into the largest arteries [17]. Tillander's research on magnetic guidance was subsequently improved to steer a catheter with an articulated tip within the heart, observe the catheter tip in the human body through imaging and design a ferromagnetic material to be embedded onto the catheter tip. Finally, his methodology was experimentally demonstrated through clinical trials carried out on several animals in 1970 [18]. Currently, "magnetic guidance" is used for magnetic catheter positioning using external magnetic fields [19], controlling the movements and positions of an ablation catheter within the heart [20], controlling intraocular micro-robots for ophthalmic procedures [11], pulling and steering endoscopic capsules in the human intestine [21] to name but a few.

Magnetic guidance techniques have played a key role in medical instrumentation related to minimally-invasive medical procedures [22, 23]. This refers to the penetration of the catheter, being a thin and flexible tube that can intervene inside of a body cavity, duct and vessels, into the heart without opening the chest [24]. A

magnetic catheter generally refers to a flexible silicone rubber tube housing the tip of the catheter, onto which one or more small magnets (or so-called magnetic seeds) are attached to the stiffer tube in the rest of the catheter [19, 25, 26]. Furthermore, it is worth noting that the magnetic seeds can be made of either hard magnetic or soft-magnetic materials and that these also partially affect the flexibility of magnetic manipulation within the whole system [27, 28]. Consequently, the key advantages of magnetically positioning a magnetic catheter inside the human body include (i) enhancement of the effectiveness of therapeutics and diagnostics, and (ii) easing the pain and trauma of patients [9].

Due to the medical benefits of magnetic guidance, there has been a variety of magnetic navigation systems designed and developed for cardiovascular applications [10, 29-31]. This thesis reports on a remote catheter tip positioning system developed specifically for steering magnetically-tipped catheters. The system employs eight electromagnets placed at 90 degrees with respect to one another. Collectively, they generate sufficient magnetic forces to accurately position the catheter tip in a desired position. This system is described in detail in Chapter 3.

The stability of the catheter tip is a challenge in a dynamic environment. To overcome this hurdle, the catheter tip must be precisely controlled to reach difficult zones within the heart before the ablation procedure takes place [32]. Consequently, an accurate model is crucial for the development of a magnetic catheter control system capable of positioning the catheter tip at arbitrary positions. A multitude of magnetic tips consisting of different structures and characteristics have been fabricated for medical applications. The forces required to drive on magnetic catheter tip, depend on the type and positions of the catheter tip magnet seeds, as-well-as the environment within which the catheter tip is operating. A comprehensive understanding of the relationship between these forces and the catheter tip structure is therefore crucial to accurately positioning the magnetic catheter.

1.3 Contributions of this study

In this thesis, a comprehensive mathematical model that predicts the motion of a three-magnet-tip catheter controlled by an externally applied magnetic field generated by an eight-electromagnet system is presented. This comprehensive

mathematical model accurately predicts the position and deflection of the three-magnet-tip catheter in the external magnetic field within a 3D workspace. Specifically, the model:

(i) Calculates the torques and forces exerted on the three seed magnets embedded into the catheter tip.

(ii) Predicts the displacement and curvature of the catheter tip.

(iii) Enables guiding the catheter tip to a desired position and along an arbitrary trajectory.

We also carry out proof-of-concept experiments to validate the simulation results predicted by the mathematical model.

1.4 Thesis outline

This thesis work is presented in 5 chapters:

Chapter 2 introduces existing remote catheter tip positioning systems and different types of catheter tips. Background which is relevant to this research, such as the principles of magnetism, magnetic torque and force calculation, the magnetic interaction force between two magnetic dipoles and the Euler-Bernoulli beam theory, is also presented.

Chapter 3 presents a detailed system description along with magnetic field modelling of the catheter tip positioning system, in the 3D workspace. A flowchart is built to present the accuracy of magnetic field calculation. Subsequently, simulation results of the externally applied magnetic field are performed through MATLAB program.

Chapter 4 focuses on the analysis of the torque and forces acting on three magnetic seeds that are attached to a catheter tip. A comprehensive mathematical model is then proposed, for the deflection and equilibrium configuration of the magnetically-tipped catheter using the knowledge and facts presented in Chapter 2 and 3. Using the model, an iterative algorithm is developed to find a new equilibrium position of the tip in the workspace. Then experimental results are shown the displacement and deflection of catheter tip steered in the externally applied magnetic field.

Finally, Chapter 5 summarizes the work, draws conclusions from the presented results and looks at the potential future development of the work.

CHAPTER 2 BACKGROUND AND LITERATURE REVIEW

This chapter starts with an introduction and discussion of well-known magnetic catheter tip positioning systems which have been developed for cardiovascular applications. These systems are all based on the same operating principle, in particular, using the externally applied magnetic field to steer the magnetically-tipped catheter. The second section provides a review of state-of-the-art magnetic catheters and provides a detailed analysis of factors that impact on the position and deflection of the types of catheter tips in the applied magnetic field. The third section describes in depth the principles and background for modelling the magnetic catheter tip positioning systems. Specifically, the published works on magnetic field modelling, along with the torque and forces acting on the catheter tip, are reviewed and discussed in a mathematical model for the displacement and deflection of the magnet catheter. These principles and theories are applied to develop a comprehensive mathematical model of the multi magnet tip catheter presented in this thesis.

2.1 Existing magnetic catheter navigation systems in the field of interventional cardiology

There is an increasing demand for remote magnetic navigation systems, especially for emerging medical applications. Specifically, studies have made significant contributions to medical innovations such as the application of these systems in ophthalmology [16], cardiology [17, 20, 33], intestinal gastroenterology [21], laparoscopy [34] and neurosurgery [35]. In terms of cardiovascular applications, magnetic navigation systems can be used to position and control the motions and deflections of a catheter's magnetic tip within a patient's heart, through the use of external magnetic fields [36]. This study specifically focuses on magnetic catheter steering systems for atrial fibrillation ablation. In recent years, a number of magnetic navigation systems have emerged and achieved significant success [29, 31]. Two main systems are considered such as the Niobe and the Catheter Guidance, Control and Imaging (CGCI) magnetic navigation system. Several main achievements of these systems can be listed such as substantially decreasing radiation exposure and total fluoroscope time in order to enhance physicians and patients safety [37, 38].

The clinical advantage of these systems is the magnetic remote control by experienced physicians and operators from adjacent control rooms. Therefore, physicians and operators are protected from standing with heavy protection suits during long periods of time [6].

2.1.1 The evolution of the Niobe® magnetic navigation system

The first generation of the Stereotaxis Niobe system was the Telstar Magnetic Guidance System (MGS) in 2002, as shown in Fig. 2.1 [26]. The operational principle of this system was the generation of controlling the magnetic fields up to 0.15 Tesla (T) for manoeuvring the position of a magnetic ablation catheter within the heart. The system consisted of three superconducting electromagnets surrounding an animal torso. A control computer was used to compute and control the appropriate electric currents flowing through each electromagnet to deflect the catheter tip in the direction of the magnetic field vector. The torque and force acting on a permanent magnet in the catheter obtained maximal values when the tip was perpendicular to the magnetic field and decreased to zero when the tip aligned with the magnetic field vectors. Experiment-based results estimated the precise navigation to be below 1mm [33]. However, the limitation of this study was that this system failed to provide real-time control. The time to activate each magnetic field manipulation is just under 20 seconds [26]. This causes high risks of vessel perforation and difficulties in navigating the catheter tip to complicated areas within the heart.

Fig. 2.1. Telstar Magnetic Guidance System from Stereotaxis, Inc. [26]

To overcome the hurdles, a next-generation Stereotaxis Niobe system was developed by Stereotaxis Inc., St. Louis, Missouri, USA in 2004 [30]. As can be seen in Fig. 2.2, instead of using superconducting electromagnets, this system applied two large

focused-field permanent magnets located on each side of the patients' torso to create a uniform magnetic field 0.08T in a spherical workspace measuring approximately 15cm and mounted on robotic arms to manoeuvre the catheter tip inside the heart [39]. The system is controlled by a click of the mouse from a control room that is adjacent to the operating room. Feedback from this system is displayed using a graphical user interface for the physicians, who can control an intravascular catheter through a joystick [31]. In addition, two permanent magnets can rotate 360^0 to (i) follow the orientation of applied magnetic field vector and (ii) simultaneously control the magnetic field gradient to navigate the catheter to the desired location.

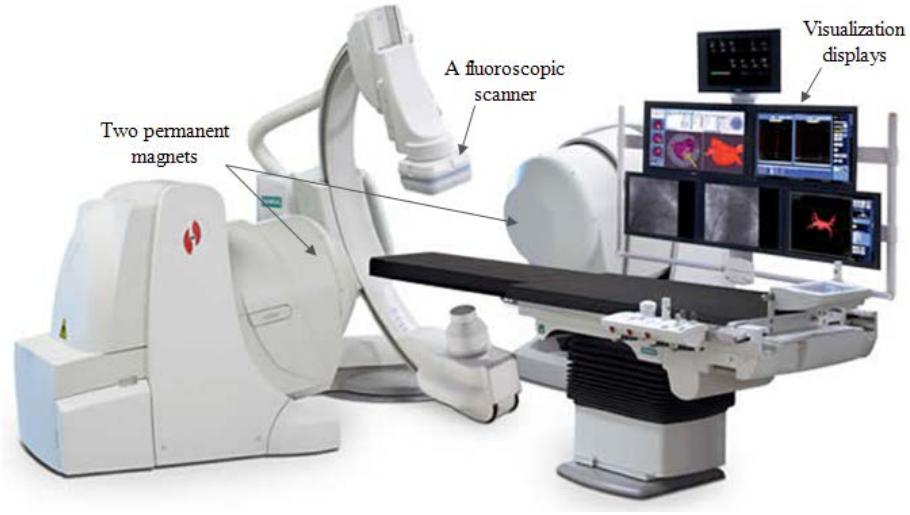

Fig. 2.2. The Stereotaxis Niobe magnetic navigation system [40]

According to the conventional technique, the Halbach approach was used to design and optimize the shape, size and material of magnets [41]. However, the Niobe system predominantly focuses on selecting the magnetic material so that the weakest field component can be maximized in the workspace where the control axes for each single magnet comprises two rotational degrees of freedom and one translation component as depicted in Fig. 2.3. Furthermore, it is also crucial to balance between the performance of the magnet, the mechanical degrees-of-freedom (DOF) and the volumetric restrictions of the design [42]. Therefore, Neodymium-iron-boron alloy was chosen to produce two permanent magnets, due to its high magnetic energy [12, 31].

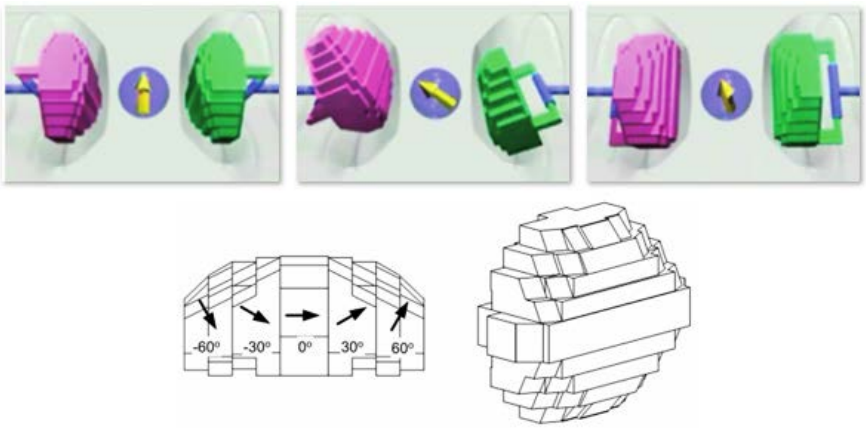

Fig. 2.3. Three figures above show that the direction of the generated field is controlled by possible arrangements of two permanent magnets in the Niobe system and each single magnet has 3 DOF (two rotational DOF and one translation component) [31]; the figure below indicates that the structure of the permanent magnet is shown as a single magnet array and magnetization orientations with different angles in the cross-section plane [42].

This system has introduced positive capabilities and benefits such as:

(i) increasing accuracy with catheter mapping and manoeuvrability

(ii) improving catheter stability with constant tissue contact [20]

(iii) decreasing fluoroscopic exposure for both patients and physicians

(iv) decreasing risk of cardiac perforation [8, 31]

However, a number of drawbacks need to be considered, these being the large size of the two permanent magnets, not being strong enough for tissue contact force, and not being able to adapt to catheter responses in real-time [14]. In recent years, the fourth generation of this system has been known as Niobe-ES. The innovative components are a graphic workstation (Navigant) in conjunction with a computer-controlled catheter advancer system (CardioDrive) in order to improve the accurate orientation of the catheter with 1-degree increments and 1-mm steps in advancement and retraction [43, 44]. According to the Stereotaxis Inc., this system has been commercialized and installed in over 164 units in the world [40].

2.1.2 The Catheter Guidance, Control and Imaging (CGCI) system

A Catheter Guidance, Control and Imaging system has been designed and developed by Magnetecs Inc. in USA. Experiments on pigs in 2011 demonstrated the innovative features of the CGCI system, such as safe, precise, closed-loop control and real-time navigation. This system as illustrated in Fig. 2.4 comprises eight powerful coil-core electromagnets that are arranged semi-spherically around the subject's torso and which generate a dynamically shaped magnetic field (up to 0.15T), concentrated on the region of the heart approximately $15cm^3$ [10, 14, 45]. The CGCI system designers have addressed the limitations of the previous systems such as rapidly changing direction, gradient and magnitude of the generated magnetic fields to provide sufficient torque and force for pushing/pulling and/or rotating/bending the magnetic catheter tip, to the desired position in real time, whilst using a closed-loop servo system to maintain the catheter tip stability [10]. The Magnetecs company also received the CE-Mark in late 2011 [29]. The CGCI system still has some challenges such as lesion visualization and shortage of real-time contact force monitoring [14]. To have a better understanding of the system, the next section presents the advantages and disadvantages of the system, when compared to the Niobe system.

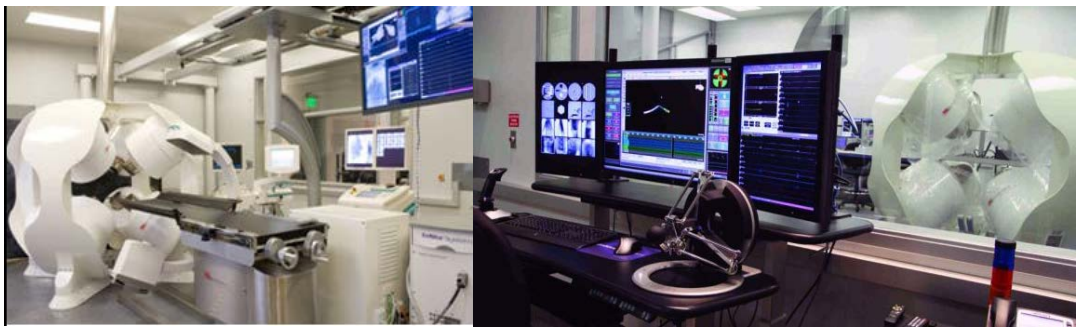

Fig. 2.4. The Catheter Guidance, Control and Imaging magnetic navigation system from Magnetecs Corp.

2.1.3 Comparison of clinical and technical specifications between remote magnetic navigation systems

There have been numerous clinical reports on the use of the Niobe and CGCI magnetic navigation systems for curing cardiac arrhythmias. Faddis et al. conducted an experiment on animals to test the accurate manipulation of the Niobe system [26]. By establishing experiments using a realistic phantom heart under various conditions,

Armacost et al. found that the accuracy for reaching the desired position was 100% [46].

According to the report on the CGCI system in 2011, Gang et al. demonstrated that (i) the repeatability of this system was 91±8.3%, (ii) the reproducibility of the system's ability to achieve the same stable point within 5 successive times was up to 96±8.4% [20], the accuracy for the final distance from the fixed catheter tip to the expected position was 1.9±0.4 mm, and (iv) the system took 11.6±3.5 seconds to reach to the designated position from the initial position of the catheter tip [10]. To better understand the benefits and limitations of magnetic navigation systems, the specifications of the two presented systems are compared in Table 1.

Characteristics	Niobe (Stereotaxis Inc.)	CGCI (Magnetecs Corporation)
Operational principle	• Two large permanent magnets	• Eight coil-core electromagnets
Commercialized	• Yes	• Yes (human clinical trials scheduled)
Cardiovascular applications	• Studies have been published in supraventricular tachycardia, atrial fibrillation, ventricular tachycardia ablation • Abilities to map and ablate in all cardiac chambers • Endocardial/epicardial mapping and ablation	• Potential for mapping and ablating all cardiac arrhythmias • Potential for all cardiac chambers mapping and ablation • Potential for endocardial/epicardial mapping and ablation
Advantages	• Perforation at a low risk level • Semi-automated mapping • Numerous clinical trials published • Catheter stability [47]	• Perforation at a low risk level • Closed loop servo system • Having the ability of integrating with a 3D-mapping system • Near real-time catheter movement • Enhancing the stability of the catheter tip. • Semi-automated and automated

		mapping • Quickly change the direction of the magnetic field without using a lot of energy • When switching the system off, magnetic field is zero. Hence, the shielding is no need.
Disadvantages	• Patients can cope with implanted devices, due to risks in command of the applied magnetic field. • Large external magnet sizes [31] • Non-real time movement • Limited to magnetic catheters • Due to the use of permanent magnets, most energy derived from them has a dispersed magnetic field. • Cost [47]	• Patients can cope with implanted devices, due to risks in command of the applied magnetic field. • Limited to magnetic catheters • Cost [29]
Future directions	• Automated mapping • Catheter technology	• Clinical assessments • Catheter technology

Table 2.1. A comparison between the Niobe and the CGCI magnetic navigation system [45]

2.1.4 Aeon Phocus system

The Aeon Scientific Company was founded in Schlieric, Switzerland in 2010 with the specific objective of developing a catheter steering system as shown in Fig. 2.5 for treating cardiac arrhythmias. This system known as Aeon Phocus, is the next generation of the magnetic catheter navigation systems based on electromagnetic manipulation technology. According to patented technology for steering the magnetic field produced by electromagnets, this system can provide ultimate dexterity and reachability within all four heart chambers [48].

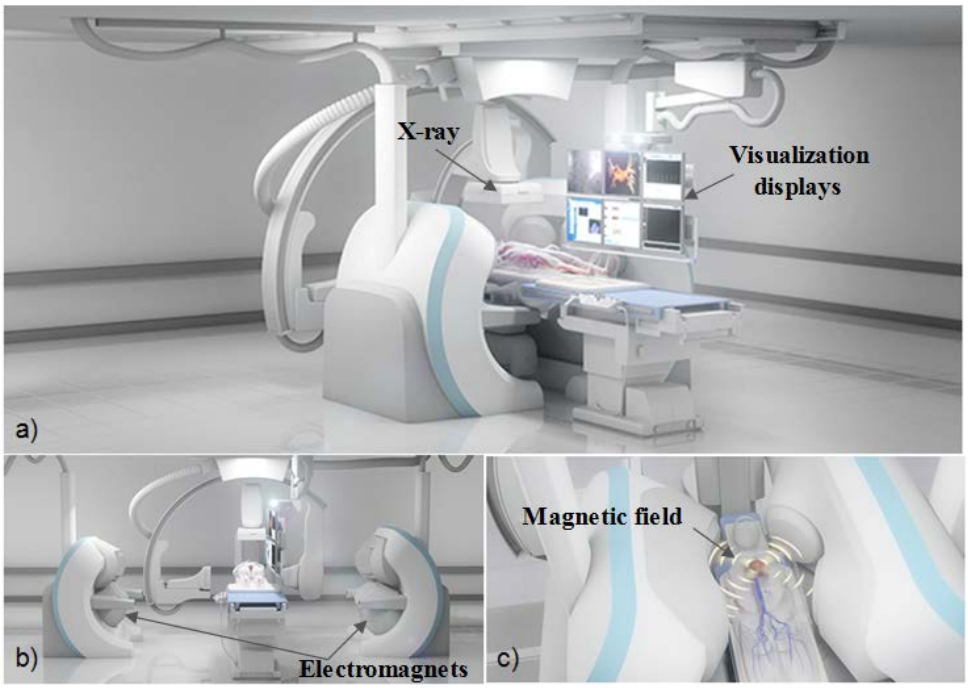

Fig. 2.5. (a) Aeon Phocus system. (b) The system consists of eight electromagnets. (c) Electromagnets generate an external magnetic field with the appropriate torque and force for moving, positioning and directing the magnetic catheter tip inside the patient's heart [48].

The objective of the Aeon Phocus is to (i) achieve the best possible intuitive control over an ablation catheter within the heart, (ii) release a device considerably smaller than existing systems, and [20] have the potential to precisely navigate the catheter, by pushing it against cardiac tissue during ablation as depicted in Fig. 2.6.

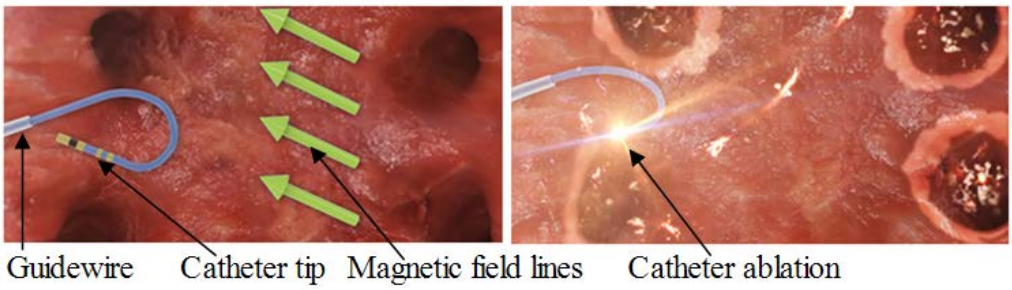

Fig. 2.6. A catheter tip is aligned parallel with the magnetic field lines and bent maximally to ablate tissues within the left atrium of the heart to treat atrial fibrillation [48].

2.2 Electromagnets in the catheter tip positioning systems

With reference to the state-of-the-art systems presented in the previous section, there are two main sources for the generation of controlled magnetic fields including (i) permanent magnets and (ii) electromagnets. Concerning the permanent magnet, its volume is in direct ratio to field strength. However, the magnetic fields produced in medical applications are required to be flexible and strong enough with respect to the appropriate volume of magnets to control the position, orientation and rotation of the magnetically-tipped catheter. Consequently, researchers have used electromagnets in recent years, because this material enables to improve simpler real-time control and quickly increase the strength of the magnetic field. In the sections below, the characteristics and benefits of electromagnets are analysed to explain why the remote catheter tip positioning system in this study, is designed and developed based on electromagnetic materials.

2.2.1 Comparison between permanent magnets and electromagnets in sources of magnetic field

It is necessary to note that permanent magnets or electromagnets has their own strong and weak points and choosing the magnetic material used in a magnetic navigation system is application dependent [12]. The eight soft iron-core electromagnets in CGCI systems seem to be the ideal solution for generating highly focused magnetic fields [13]. In more detail, the external magnetic field generated from the electromagnets (0.16 Tesla) is stronger than the one produced from two massive permanent magnets in the Niobe system (0.08 Tesla). Moreover, it is important to note that electromagnets can navigate the catheter tip to desired positions by adjusting the magnitude of the electric currents flowing through the coil-core electromagnets. Conversely, permanent magnets produce fixed magnetic fields without controlled electric currents and guide the catheter tip by varying the distance and rotation of the two permanent magnets [30]. In addition, long soft-magnetic cores placed inside electromagnets make the magnetic field considerably stronger and more concentrated. Electromagnets are also easily magnetized and quickly lose their magnetism when the currents are switched off. This helps the system to be safe in medical environments. As a result, electromagnets are able to quickly and continuously shape and reshape the magnetic field, rather than rotating and moving

two large permanent magnets to change the magnetic field [30, 49]. This considerably improves the stability of catheter tip. As a result, the CGCI system has achieved significant results in accurate control and mapping, flexibility in bending the catheter tip, and real-time response [14]. Briefly, the important characteristics of electromagnets and permanent magnets are compared in Table 2.2.

Features	**Materials**	
	Electromagnet	**Permanent magnet**
Field strength	Varying	Fixed
Magnetic field	Variable	Permanent
Geometry	Complex	Simple
Energy	Requires energy	No energy needed
Temperature	Produce heat	Sensitive to heat
Cost	Expensive	Cheap
Control technique	Electronically controlled	Mechanically controlled

Table 2.2. Comparison of material characteristics between electromagnet and permanent magnet [9].

2.2.2 Advantages and challenges of using electromagnets in generating a magnetic field

To design a powerful electromagnetic system, some key factors need to be considered, such as (i) the number of electromagnets to be used, (ii) how the electromagnets should be arranged in the system and how the magnetic field is to be generated [20]. Specifically, multi-magnet systems increase degrees of freedom with the objective of precisely and flexibly controlling the catheter tip in any direction [12]. According to the comparison between the experimental results of system geometries [12], it depends on the various individual applications to determine the number of electromagnets and the orthogonal electromagnetic arrangements with the aim of precisely manoeuvring the catheter tip. In this study, the catheter tip positioning system is designed using an arrangement of eight electromagnets.

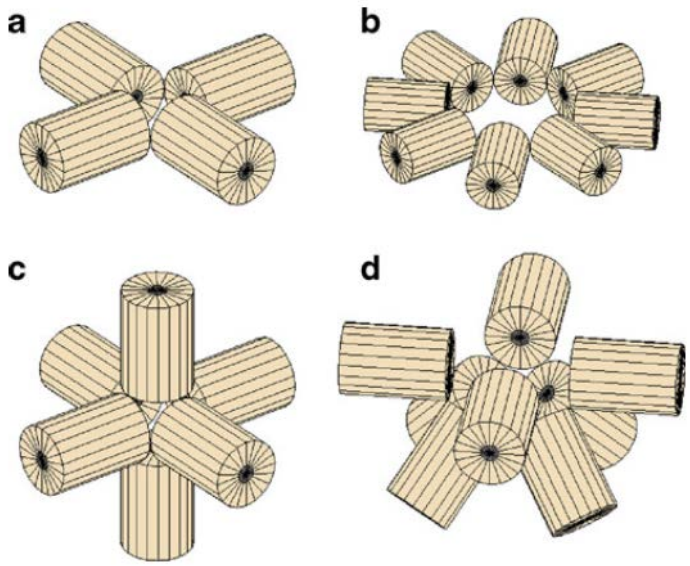

Fig. 2.7. Electromagnet arrangement in magnetic steering systems. a) A two-dimensional four-magnet system includes two pairs of opposing magnets arranged orthogonally at 90◦. b) Likewise, eight magnets with angles of 45◦ between them in a two-dimensional workspace. c) Three pairs of opposing electromagnets are placed on the axes of a Cartesian coordinate frame in a three-dimensional workspace. d) OctoMag electromagnetic system with eight magnets arranged as above [12].

When the number of magnets is increased, the ability to manoeuvre the magnetic field improves [12]. The Octomag system, Fig. 2.7(d), can be taken as an example to illustrate the creation of an isotropic workspace with uniform magnetic fields. This configuration simplifies modelling and control [11, 12]. In addition, the electromagnets need to satisfy the practical design criteria [50], in this respect, the eight iron-core electromagnet system can obtain the same field strength at each coil to keep the magnetic catheter tip stable. In practice, magnetic fields are likely to be nonlinear in operation and this becomes a challenge for calculating magnetic torques and forces on magnetic objects. As such, the design of a magnetic core is also taken into consideration as part of the problem solution. Particularly, the coil can be designed with an extendable core which shapes the magnetic field characteristics and creates a focused magnetic field strength through energized electric currents [15]. As a result, it is important to design appropriate alloys with high performance soft-magnetic materials to enhance the magnetic field strength [11, 12].

Coil design refers to the arrangement of current-carrying wires designed to generate a prescribed magnetic field through an applied electric current [51]. When the catheter tip is magnetically controlled in the cardiovascular system, the generated magnetic field is required to be strong and accurate. The magnetic field strength depends on factors such as (i) the number of turns of wire within the coil, (ii) the amount of current flowing in the coil, [20] the type of core material and (iv) length of the core inside the coil [52]. In this study, electromagnets are chosen for the remote catheter tip positioning system for magnetic manipulation instead of superconducting materials. Superconducting materials are not suitable for the following reasons:

- The electric flux flowing through superconducting coils is much more than that of copper coils, which results in enormous power consumption.
- It is not practically feasible to employ liquid helium cooling which is required for most superconductors.
- It is hard to quickly vary currents needed for high-bandwidth real-time control.

For these reasons, superconducting coils are unlikely to be an optimal method for magnetic navigation systems. As such, coils winded by copper wire are most frequently used due to their low electrical resistance and reasonable heating and cooling [12].

2.3 State-of-the-art magnetic catheters

The design of steerable catheters has improved over many years. Tillander, who was the first to use a magnetic catheter in 1951, applied a large external magnet to magnetically guide the catheter into the largest arteries [17]. Tillander's research on magnetic guidance was subsequently improved to steer an articulated steel-tip catheter within the heart [18]. Research has shown that the outer environment and structural characteristics of a catheter are considered to be major factors in designing coils and catheter tips in order to optimize catheter manipulation and reduce power consumption [25].

A wide range of radiofrequency ablation catheter tips has been published in recent decades, with the designs improved to gain smooth transition and accurate manoeuvrability [53]. Fig. 2.8 shows some typical magnetic catheters used in magnetic catheter navigation systems. The initial ablation bipolar catheter (Helios I,

Stereotaxis) had a single magnet with 8F diameter in the distal tip. This catheter tip was limited by the stiffness of a long magnet [5, 7, 8]. In the subsequent years, the 8F-diameter ablation catheter (Helios II, Stereotaxis) was improved by integrating three magnetic seeds and two electrodes into the catheter tip so that catheter manipulation had smoother transitions and increased deflection via magnetic navigation [7, 54]. Next, the improved 7F-diameter ablation catheter had 4 electrodes (quadripolar) and three magnets attached to the catheter tip [5]. A magnetically guided irrigated gold-tip catheter was designed and produced with 3 magnetic seeds and 4 gold electrodes in the distal tip. This was because the thermal conductivity of gold is approximately four times greater than platinum-iridium and irrigated tip electrodes, with saline solution, can actively cool at the tissue interface [55]. This irrigated tip catheter was combined with a CARTO location sensor in order to perform both mapping and ablation through remote control [56]. Importantly, the first research into evaluating the feasibility and safety of this catheter tip for ablation of AF gave results that demonstrated its benefits [57].

The constraints in designing catheter tips are based on parameters such as the length, diameter and materials of the electrodes and seed magnets, electrode and seed magnet spacing, as well as the number of seed magnets and electrodes [55]. It is essential therefore to precisely compute the parameters of magnetic navigation systems and magnetic catheters in order to correctly design them. Certification for use in clinical applications is a lengthy process and requires multiple experiments on animals prior to trials on patients. The predominant challenges in designing the system can be taken into account with the cost of steerable technologies, miniaturization and control [6].

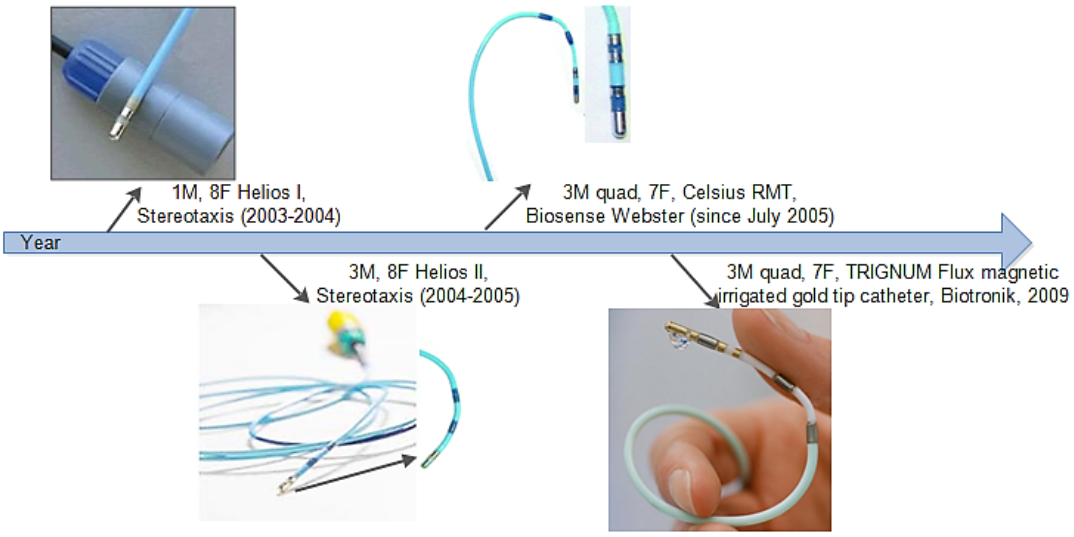

Fig. 2.8. The evolution of typically magnetic catheter tips in the field of endovascular catheterization.

2.3.1 The effects of seed magnet structure on catheter tip deflection

In an experiment on three patient groups in 2007, magnetic remote-controlled accessory pathway ablation was performed by using the Niobe system to control three types of magnetic catheters in patients. Researchers assessed the safety, feasibility and effectiveness of the catheter tips through practical measurements [5]. Specifically, the catheters were equipped with a different number of permanent magnetic seeds in their distal tips. As illustrated in Fig. 2.9, the first catheter had a magnet on its distal tip, the second one had a bipolar 3-magnet tip and the last one had a quadripolar 3-magnet tip. The three different types of magnetic catheters were trialled on three patient groups. The experimental results of the 3-magnet quadripolar ablation catheter showed that it had the highest percentage of successful ablations. The authors also considered enhancing the ability to control catheter tips precisely and efficiently by investigating the impact of the number ,size and spacing the of small permanent magnets .[5]. The magnetic seeds embedded in the catheter tip should have appropriate length and spacing to improve the catheter movement and make the motion smoother. [7].

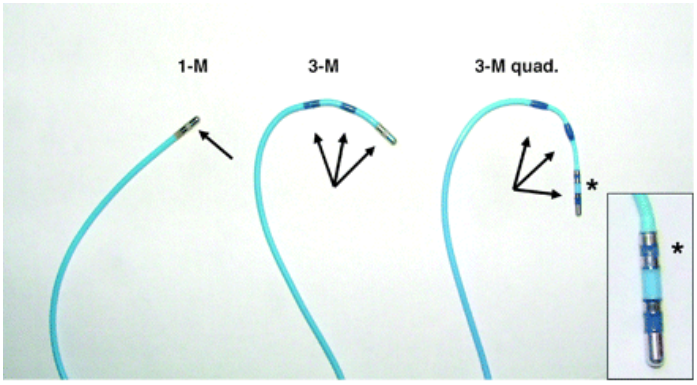

Fig. 2.9. Three types of catheters applied to experiments on three patient groups [25]

At the same time in 2007, an experiment was implemented by using the Niobe system to demonstrate the accuracy and actual displacement of the 3-magnet quadripolar ablation catheter from a desired target position. Specifically, the magnetic deflection tester (MDT, Stereotaxis, Inc.) was used to test the deflection of this magnetic catheter. The discrepancy between the observed angular deviation of this catheter and the predicted value was under 4^{o}. In addition, it was found that the measured tolerance of the catheter movement fluctuated at the desired positions to within 1 mm. This precision ensured that the Niobe magnetic navigation system had the potential to achieve high success, with low risk rates of cardiac catheterization [46]. Consequently, the distance from the current position of the catheter tip to the desired target must be measured to advance or retract the catheter tip with the appropriate lengths as illustrated in Fig. 2.10. Significantly, there is a correlation between the curvatures of the catheter tip and the number of seed magnets attached to the catheter tip. If the number of magnetic seeds increases, the transition of the catheter tip is smoother and the bending angle of the tip is broader to accurately steer to expected positions in difficult regions of the heart. In other words, increasing the number of magnetic seeds increases the number of degrees of freedom (DOF) for the catheter so that the catheter tip moves flexibly in pulmonary veins [46].

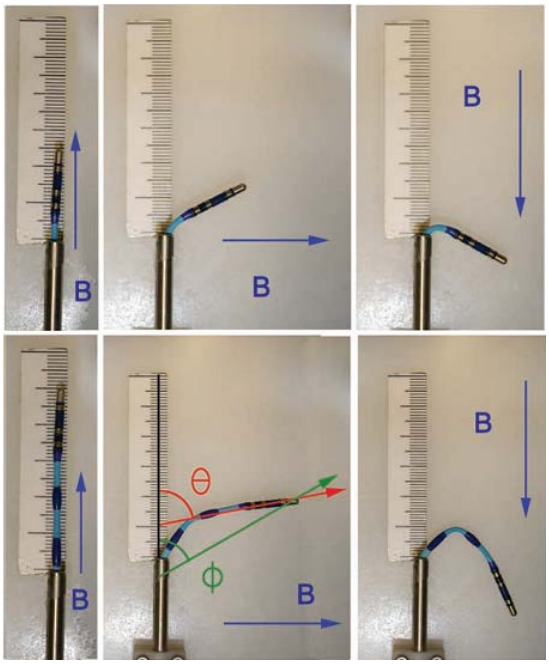

Fig. 2.10. The curvatures of the catheter tip are measured in an external magnetic field B. As can be seen from the first row, the deflection angle of the catheter tip is quite minimal with the orientation of B at 0^o, 90^o, 180^o respectively and the length of the tip is extended 2.5cm. With regards to the second row, the deflection angle of the catheter tip is larger with the orientation of B at 0^o, 90^o, 180^o respectively and the length of the tip is extended 5cm. A magnet is put in each dark blue section attached to the catheter tip [46].

2.3.2 Properties of hard or soft magnetic seeds for steering the catheter tip in the external magnetic field

Many magnetic catheters have been designed by researchers to meet the strict requirements of catheter manoeuvrability [53, 58]. In this study, the magnetic seeds are small compared to the variation of the applied magnetic field in the 3D workspace. Consequently, the magnetic flux density can be assumed to be sufficiently uniform across the magnetic catheter. This assumption has been validated through experimental results to predict precisely the magnetic torque and force [28, 59]. The different shapes of magnetic seeds have different magnetization, in spite of their hard or soft magnetic materials [27]. The advantages and disadvantages of hard magnetic materials and soft magnetic materials will be presented in order to facilitate selection for magnetic seeds.

2.3.2.1 Hard magnetic material

When using a permanent magnetic material to produce seed magnets, the magnetization (M) of this material is independent of the generated magnetic field and these seeds can be modelled as magnetic dipoles. This simplifies the process of calculating the torque and force, if the two parameters $\vec{m}$ and $\vec{B}$ are known. The magnetization of permanent magnets is dominated by the remanent magnetization of the material and the geometric shape of magnetic seeds. To increase the torque, the angle between $\vec{M}$ and $\vec{B}$ can be adjusted incrementally up to 90^{o}, or alternatively enhance the magnetic field strength. To increase the force, the magnetic gradient can be increasingly varied in the applied field [27]. When the magnetic catheter tip is inserted into the body, this requires a maximum magnetic field strength in a minimum volume. Permanent magnets are therefore a better candidate than electromagnets in this context.

2.3.2.2 Soft magnetic material

Unlike a permanent magnetic material, the magnetization of the magnetic seeds made from a soft-magnetic material is a nonlinear function of the applied field. This material can be fabricated with different possibilities of control. The magnetization of soft magnetic materials can also be obtained at high levels matching the remanent magnetization of permanent magnets [60] and it depends on the strength and the direction of the magnetic field. However, the field possesses a magnitude that is limited by the saturation magnetization for the magnetic material and can also rotate with respect to the seeds [27]. The correlation between the applied magnetic field and the resulting torque and force must be controlled, since the force depends on key factors including the spatial gradient, the strength, and the direction of the magnetic field. Hence, it is more complicated steering the catheter tip when it is constrained by many variables as mentioned above.

2.4 Magnetic field modelling

The previous sections have provided an overview of remote magnetic catheter navigation systems as-well-as different types of the magnetic-tipped catheter. In the next three sections, magnetic field modelling, the calculation of magnetic torques and forces acting on the catheter tip, and theories of electromagnetic field and elasticity

will be presented. Based on these reviews and theories, a comprehensive mathematical model for the catheter tip positioning system in this thesis will be developed in the following chapters.

A considerable amount of literature has been investigated and published on magnetic field modelling. Two magnetic field models are discussed below due to the similarity of using electromagnets. In 2010, the Octomag system, which was defined as the electromagnetic system for 5-DOF (3-DOF position and 2-DOF pointing orientation) wireless micromanipulation, was developed and published by Bradley Nelson and his colleagues at ETH Zurich [11]. Essentially, the Octomag system controls untethered magnetic microrobots through an externally applied magnetic field. The eight soft-magnetic-core electromagnets, shown in Fig. 2.11, create magnetic fields that control the microrobot. However, the Octomag system also has difficulties with the ability to apply large forces and to bring large payloads due to the tiny size of the microrobot. This system achieves precise control of a wireless microrobot through closed-loop position control using computer vision. More importantly, the system is based on visual feedback without visual tracking, thus it can send the position of the microrobot to the operator during the teleoperation process. In addition, this system makes use of complex non-uniform magnetic fields to control fully untethered microrobots. With appropriate modification, a similar system can be developed for tethered devices such as magnetic catheters and guidewires [11].

Fig. 2.11. The Octomag system contains eight soft-magnetic-core electromagnets and in the central space of eight electromagnets is the untethered microrobot [11].

To model the magnetic field, Kummer et al. [11] built a unit-current field map for each electromagnet by using finite-element-method (FEM) models in order to

measure the magnetic field of this system or calculate the magnetic field values at grid points. Consequently, this model predicted the generated magnetic field throughout the 20mm × 20mm workspace. To expand to a larger workspace, a trilinear-interpolation method could be applied during real-time control. However, another approach used in the Octomag system to create the unit-current field map for each electromagnet was the point-dipole model. By using analytical functions in MATLAB, the complicated magnetic field of this system has been accurately modelled in the defined workspace. Additionally, due to the geometrical symmetry of the given electromagnet configuration as shown in Fig. 2.11, homogeneous transformations were applied to calculate the generated magnetic field at any point in the workspace.

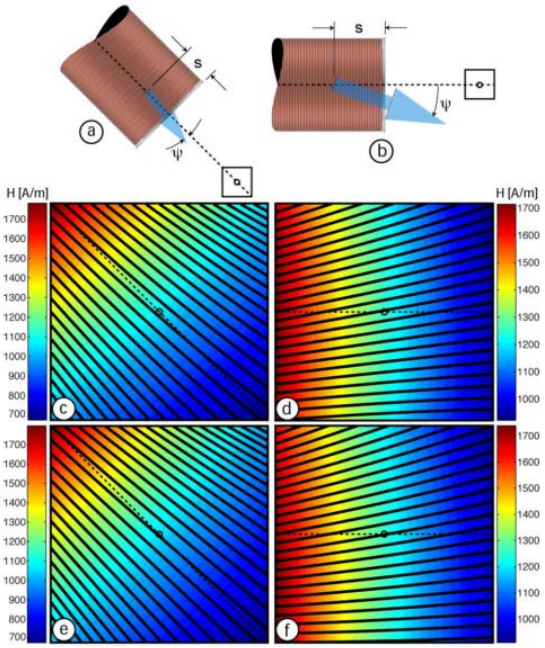

Fig. 2.12. A point-dipole model simulates the unit-current field contribution of (a) an upper electromagnet and (b) a lower electromagnet, by using the Finite Element Method (FEM). Figures (c) and (d) present FEM data for the cross-sections of the magnetic field generated from the electromagnet within the 20 mm × 20 mm workspace. Figures (e) and (f) indicate point-dipole models fit to FEM data along the electromagnet's axis, which is shown with a dotted line. The colour bars represent the magnitude of the magnetic field. The common centre of the electromagnets is shown with a circle. It is obvious that the other soft-magnetic cores affect the field, as it does not point along the electromagnets axis (c) to (f) [11].

In 2011, magnetic fields were dynamically shaped using the CGCI system. This hypothesis was validated through initial experiments on animals [10]. The simulation of the total magnetic field produced from the eight-coil electromagnetic system was demonstrated as in Fig. 2.13 and in some patents [10, 13, 15]. However, little attention has been paid to mathematical models for the total magnetic field of this system as well as the deflection of the catheter in these publications. Therefore, this thesis has developed a comprehensive mathematical model for both of them as presented in Chapter 3 and 4.

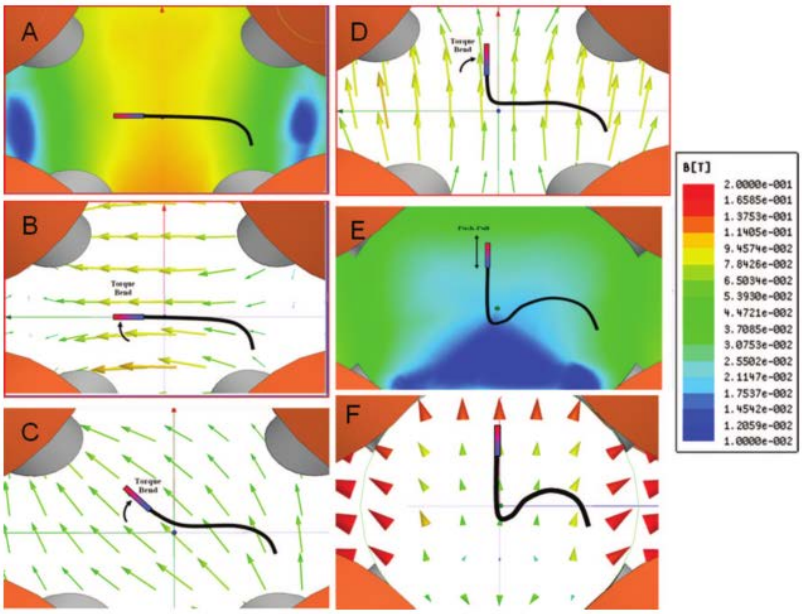

Fig. 2.13. The motion and deflection of the catheter tip in the uniform distribution of the magnetic field strength with the colour bar indicating magnetic field intensity. In Figures (A) and (B), the catheter tip is aligned with the direction of the vector field. With Figures (C) and (D), the catheter tip is rotated at 45° and 90° angles respectively to the orientation of the vector field. In Figures (E) and (F), when the magnetic field intensity is varied by electric currents, the catheter tip is pulled in the direction of the field strength, in this case, it moves vertically upward [10].

2.5 Calculation of magnetic torques and forces

This section reviews the analytical calculation of the magnetic forces and torques acting on the magnetically-tipped catheter. In the previous years, these mathematical models were limited by the number of magnetic seeds and precise external magnetic field [19, 61].

2.5.1 Modelling magnetic torques and forces acting on the one-magnet tip catheter

According to the mathematical model for a permanent magnetic seed attached to the catheter tip in the Niobe system, calculating the magnetic torque and force exerted on the seed was solved as follows. Firstly, the magnetic dipole moment m of the entire cylindrical magnetic seed was written as:

$$m = \iiint_{Vol} MdVol = MAL \tag{1}$$

where M denotes the magnetization of a permanent magnetic seed, A is a cross-section, and L is a length of the seed.

As an observation in Fig. 2.14, the magnetic torque was written as

$$T = m \times B = mB\sin(\gamma - \theta) \tag{2}$$

where γ denotes the initial angle between vectors m and B, θ is the angle between the tangent to the curved catheter and the initial horizontal axis of the catheter tip, and $\gamma - \theta$ is the final angle between m and B. In this catheter model [31], the torque was schematized and calculated through a force $2F$ acting on the tip or an equivalent couple of forces F and it was expressed as

$$T = 2FL \tag{3}$$

Substituting Eq. (1) and (2) into Eq. (3), the magnetic force was written as

$$F = \frac{1}{2}MAB\sin(\gamma - \theta) \tag{4}$$

Based on the Eq. (3) and (4), the catheter tip obtains the equilibrium configuration, when the direction of vectors B and m are aligned or the angle θ, between the tangent of the distal tip and the horizontal axis, is equal to the angle γ, between the magnetic orientation and the horizontal axis. For this reason, the magnetic torque is null and the force plays a dominant role in steering the catheter tip. Furthermore, due to the stiffness of the catheter tip, it tends to return to the straight, stress-free state without the applied magnetic field. This means the magnetic torque is against elastic recovery forces created by the flexible rigidity of the catheter structure. This makes an impact on the deflection of the catheter tip to reach a new equilibrium position.

In this research, Tunay assumed that the catheter tip made contact with the tissue. To solve the equilibrium configuration of the catheter tip in this assumption, the

principle of stationary potential energy was applied to determine the equilibrium position of the catheter tip [11, 19]. In particular, the total potential energy was taken as the sum of the strain potential energy of the catheter body U_s, the magnetic potential energy U_m and the strain energy of the deformed tissue U_t [19]:

$$U = U_s + U_m + U_t \tag{5}$$

In 2004, Tunay [19] reported the use of Newton's method, Jacobi elliptic functions and elliptic integrals to solve the boundary value problem (BVP). Since MATLAB software package has these methods built in, it was logical to use them to solve the boundary value problem for simulating the catheter position. Nevertheless, the first limitation of this catheter model has not shown the simulation results from the methods suggested [19]. Secondly, the drawback is the length of the magnetic seed posed challenges for the deflection of the catheter tip to reach complex regions within the heart [31]. Consequently, research undertaken in this area aimed to improve the efficacy of the catheter tip such as interleaving more magnets inside the distal tip [19]. Similarly, Settecase et al. [62] [62], simplified the equation and data fitting for a structurally different but magnetically equivalent system. In more detail, the equilibrium catheter deflection angle θ can be obtained by satisfying the relation:

$$\frac{\theta}{\sin(\gamma - \theta)} = \frac{MALBl}{EI} \tag{6}$$

where l denotes the length of part out of the guidewire, E is the Young's modulus of the catheter material and I is the area moment of inertia. However, this equation is still valid if it meets the following implicit hypotheses

- The distal tip of the catheter has no contact with the surrounding tissue and it is steered in free space.
- The magnetic field needs to be uniform around the seed.
- The bending stiffness EI of the catheter tip is constant.
- Forces arising from the fluidic environment such as drag or damp forces are neglected.

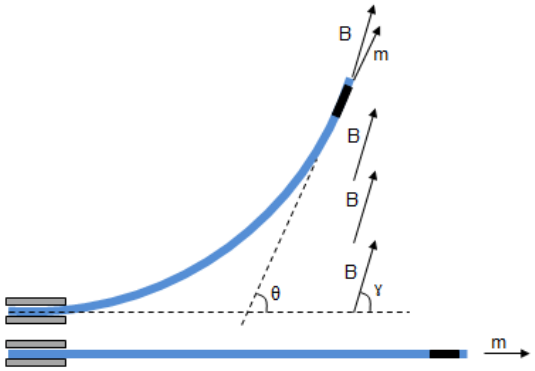

Fig. 2.14. Magnetically controlled flexible catheter with a permanent magnetic seed attached to the distal tip is extended from a guidewire [31].

2.5.2 Modelling magnetic torques and forces acting on the two-magnet tip catheter

It is worth noting that by using several magnetic seeds is possible to increase the degrees of freedom for positioning the catheter tip at desired positions. The problem however, is to find the optimal spacing between magnets. For another catheter model reported in [61], the fundamental principle of the magnetic catheter control was based upon the variation of magnetic field gradients generated from a system of high gradient coils in order to control ferromagnetic spheres integrated into the catheter tip. This is illustrated in Fig. 2.15.

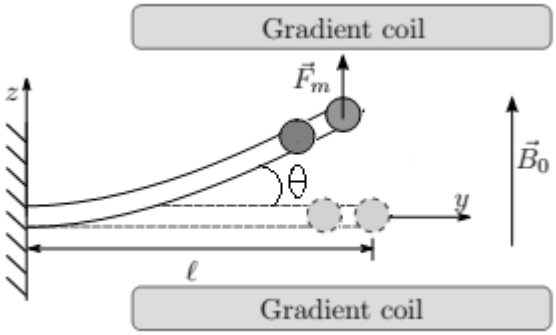

Fig. 2.15. Model of the deflection of the catheter tip based on the magnetic interactions between two Maxwell coils and two ferromagnetic spheres embedded into the catheter tip [61].

The main purposes of this model were to maximize the curvature of the catheter tip and minimize its size so as to insert it into the complex network of blood vessels. To achieve the aims, the calculation of torques and forces acting on the different types of

the catheter tip, shown in Fig. 2.16(a), was developed [61]. Besides, the impact of dipole-dipole interactions on the catheter movement was also investigated. It is generally accepted that modelling magnetic torque and force acting on the two-magnet tip catheter is more complicated than the one-magnet tip mentioned above. Moreover, the spacing between magnetic spheres placed into the catheter tip was appropriately computed for each type of catheter tip in order to obtain the optimal deflection and displacement of the tip. Experimental results have demonstrated that the tip deflection increases, when the spacing between two spheres is reduced as shown in Fig. 2.16.

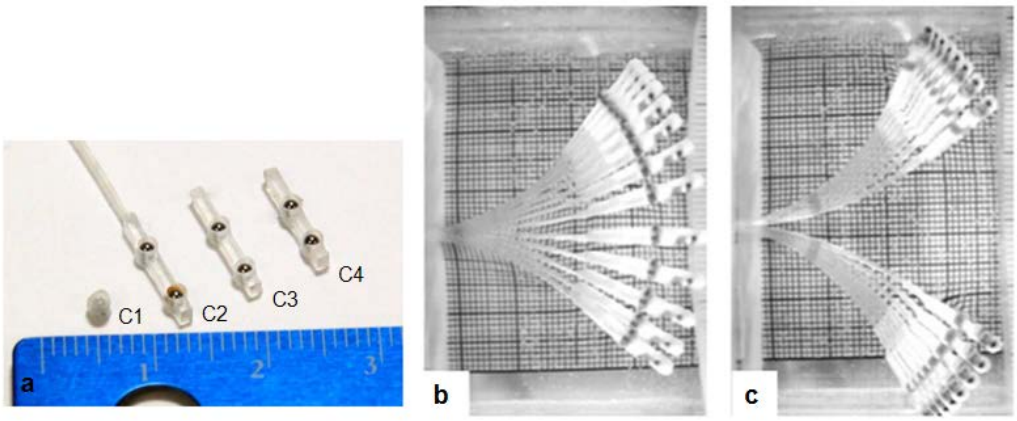

Fig. 2.16. (a) Four types of ferromagnetic catheter tips C1, C2, C3, and C4 and the number of magnetic spheres attached to the tips is 1, 2, 2, and 2 respectively. (b) and (c) The various deflections of two tips C2 and C4 are subjected to a gradient incremented from -352 to 352 mT/m. Note that C2 and C4 have the spacing 6 mm and 4mm with the free length 32 mm and 32.7 mm in the same order [61].

2.6 Theories of electromagnetic field and elasticity

Before the analytical calculation of the externally applied magnetic field and forces acting on the catheter tip is executed, the fundamental theories related to electromagnetic field and elasticity need to be investigated.

2.6.1 Biot-Savart law and superposition principle

The eight iron-core electromagnets in this system comprise two main parts: coils and iron cores. With regards to a coil, current-carrying wires can be defined as many current loops wrapped around the magnetic core of the coil. The magnetic field produced at a point P by each current loop can be computed by using the Biot-Savart

law and the superposition principle [52, 63, 64]. In particular, the current loop is divided into many current elements and each current element is considered as an arcs length $d\vec{l}$ as illustrated in Fig. 2.17. Therefore, the magnetic field $d\vec{B}$ created by a length element $d\vec{l}$ of the current loop carrying a DC electric current I to a point $P(x_P, y_P, z_P)$ is expressed as follows:

$$d\vec{B} = \frac{\mu_0 I}{4\pi} \frac{d\vec{l} \times \vec{r}}{r^3} \tag{7}$$

where $\vec{r}$ denotes the vector directed from $d\vec{l}$ toward the point P, $r = |\vec{r}|$ is the distance from $d\vec{l}$ to P, and $\mu_0 = 4\pi \times 10^{-7}$ T.m/A is the permeability of free space.

It is important to note that the Biot-Savart law is only applied for a small element of the given current-carrying conductor to calculate the magnetic field. Therefore, the superposition principle is used to sum up the infinitesimal contributions $d\vec{B}$ in order to calculate the total magnetic field $\vec{B}$ at any point P due to a conductor of finite size. In other words, the integral taken over the contribution of individual current elements in the entire current-carrying conductor is written as:

$$\vec{B}(P) = \frac{\mu_0 I}{4\pi} \oint \frac{d\vec{l} \times \vec{r}}{r^3} \tag{8}$$

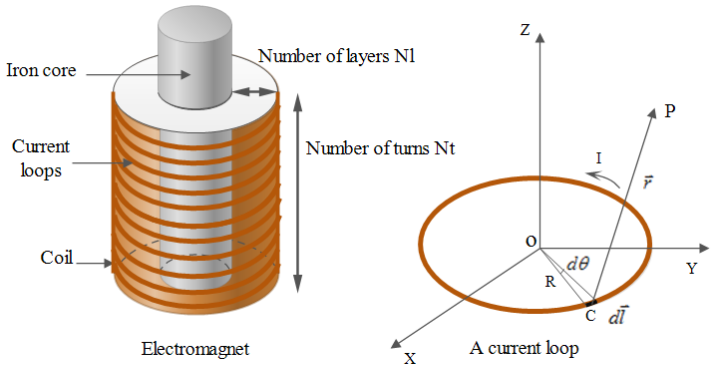

Fig. 2.17. Partitioning a current loop to calculate the magnetic field

2.6.2 Magnetic torque and force

When a magnetic-tipped catheter is placed in an externally applied magnetic field and gradients, the position, curvature and orientation of the tip can be controlled in the 3D workspace. Basically, the tip is displaced and bent in the total magnetic field $\vec{B}$, as the magnetic torque ($\vec{T}$) and force ($\vec{F}$) are exerted on three magnetized seeds with their uniform magnetization $\vec{M}$ (A/m) and volume V(m^3). As a result, the

magnetic torque (N.m) aligning magnetic seeds embedded in the catheter tip with the applied magnetic field is defined as [19, 27, 65]

$$\vec{T} = V\vec{M} \times \vec{B} \tag{9}$$

where m (A.m^2) is the magnetic moment of each magnetic seed with $\vec{m} = V.\vec{M}$.

Maxwell's equations provide the constraint $\nabla_B \times B = 0$ when the region occupied by the catheter tip has no electric current flowing through it. Therefore, the force $\vec{F}$ (N) pulling the catheter tip in the direction of the field gradient to a local maximum is given by [27]:

$$\vec{F} = (\vec{m}.\nabla_B)\vec{B} = \nabla_B(\vec{m}.\vec{B}) \tag{10}$$

where ∇_B is the gradient operator, expressed as follows:

$$\nabla_B = \left[\frac{\partial}{\partial x} \quad \frac{\partial}{\partial y} \quad \frac{\partial}{\partial z}\right]^T \tag{11}$$

From Eqs. (10) and (11), the magnetic force in any given direction is regarded as the dot product of the derivative of the field in that direction and the magnetization of the seed, we have

$$\vec{F} = V\left[\frac{\partial\vec{B}}{\partial x} \quad \frac{\partial\vec{B}}{\partial y} \quad \frac{\partial\vec{B}}{\partial z}\right]^T \vec{M} \tag{12}$$

According to Eq. (12), it is observed that the magnetic force depends on the spatial gradient of the magnetic field and consequently, the magnetic field is also governed by its magnitude and direction. For accurate catheter tip control, it is important to optimize the direction and magnitude of the external magnetic field in order to drive the seed magnets with the appropriate forces and torques needed to position the catheter tip along the desired direction and at the intended position [66]. It is important to note that the magnetic seeds are not only subjected to the external field, but are also dependant on the elasticity of the catheter body. This complicates the solution to the equilibrium configuration of the catheter tip in the applied field, when the tip is equipped with multi magnets. The Euler Bernoulli theory, presented below, with its assumption in the case of a long thin beam is used to develop a mathematical model for the catheter tip with multi magnetic seeds.

2.6.3 Euler Bernoulli beam theory

The catheter is made from elastic materials, so it can recover its initial position and status when the applied magnetic field is removed. In this study, the catheter has a long thin body with a diameter that is much smaller than its length as illustrated in Fig. 3.1. Thus, the Euler-Bernoulli model can be applied to simulate the mechanics of a beam under bending. The Euler-Bernoulli model assumes that the cross-section of the catheter tip rotates around a neutral surface remaining plane, the cross-section remains perpendicular to the neutral surface during deformation and it is also assumed that the shear deformation is negligible [19, 67-70]. In other words, this beam can be considered as a cantilever beam that is fixed at one end and is free at the other [71]. The Euler-Bernoulli equation of the beam can be expressed as [19]

$$\kappa = \frac{d\varphi}{ds} = \frac{M(s)}{E(s)I(s)} \tag{13}$$

where ds denotes the arc length of the catheter with s = 0 at the sheath and s = L at the tip, φ is the angle between the x-axis and the tangent to the curvature of the catheter as described in Fig. 2.18. From the Eq. (13), κ denotes the curvature of the beam, $M(s)$ is the bending moment perpendicular to the plane, and $E(s)$ denotes the modulus of elasticity in tension and $I(s)$ is the area moment of inertia.

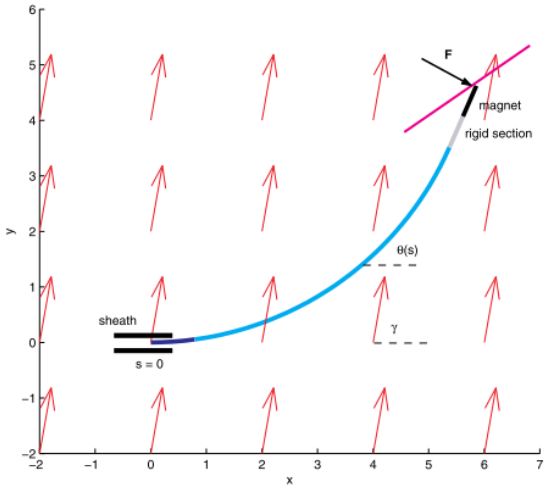

Fig. 2.18. A one-magnet tip catheter in an externally applied magnetic field [19]

2.7 Summary

In this chapter, we have discussed the foundation of many important concepts which helped the remote catheter tip positioning systems to be recognized as one of the most promising technologies of today and for future generations to come. The

characteristics, advantages and disadvantages of these state-of-the-art magnetic catheter navigation systems such as the Niobe system (Stereotaxis Inc.), the CGCI system (Magnetecs Corp.), the Aeon Phocus system (Aeon Scientific Company) were presented. According to the literature on these systems, the shortcomings of the Niobe system have been addressed by the CGCI and Aeon Phocus systems. Consequently, electromagnets are likely to be considered as an ideal solution for navigation because of their capabilities to control strength, polarity and shape of the applied magnetic field. Nonetheless, the heating of electromagnets is still a drawback, and catheter manipulation in a very dynamic environment is extremely challenging.

Radiofrequency catheter ablation has become a commonly used and well established procedure to provide a therapeutic option for patents [72], with typical catheters reviewed. Catheters are typically equipped with one magnet, two magnets, or three magnets on the distal tips. Based on advanced development in catheter design, it is generally accepted that the number, spacing, shape and size of magnetic seeds have considerable influence on the displacement and deflection of the catheter tip in externally generated magnetic fields. Moreover, the analytical calculation of torques and forces acting on the multi-magnet tip catheter plays an indispensable role in accurately positioning the catheter at desired positions.

In the following chapters, a detailed description of the catheter tip positioning system used in this study is introduced. Subsequently, modelling the external magnetic field of this developed system in the 3D workspace, the displacement and curvature of the catheter tip in the applied magnetic field based on the literature discussed earlier will be addressed. To recognize the precise position of the catheter tip in the workspace, the analysis focuses on torques and forces acting on the three-magnet tip catheter through the magnetic manipulation of modelled system. In addition, an iterative algorithm for finding the equilibrium position of the catheter tip corresponding to the increment of electric currents will be developed. Finally, the motion of the catheter tip will be verified using the developed electromagnet system to observe its behaviour in the 3D magnetic field.

CHAPTER 3 MODELLING THE EXTERNALLY APPLIED MAGNETIC FIELD

Magnetic field modelling of the catheter tip positioning system refers to the formulation of the magnetic flux density distribution of each electromagnet in the 3D workspace. Modelling the externally applied magnetic field of this system has two main purposes. Firstly, torque modelling is necessary for position and velocity control of the system. However, before computing magnetic forces and torques acting on the magnetically-tipped catheter, it is necessary to calculate and simulate the external magnetic field distribution of eight iron-core electromagnets in the central magnetic region of the system. Secondly, the magnetic field model facilitates the simulation and comprehension of the flux density variation of eight electromagnets. The following sections in this chapter describe the system and the analytical solutions and simulation results of the magnetic field modelling.

3.1 System description

The proof-of-concept catheter tip positioning system demonstrator, shown in Fig. 3.1, was developed in collaboration with PointPlace Ltd-Australia, and Hunan Forever Elegance Technology - China. The electromagnet system has been designed by another ESRI group. This research project focuses on the development of the mathematical model for driving this system and demonstrating its ability to control a 3-magnet-seed catheter tip. This demonstrator comprises 8 electromagnets placed in 3D at 90 degree angles with respect to one another. It was designed to generate a magnetic field of up to 0.15 Tesla within a central volume of 128mm×128mm×128mm by controlling the eight electric currents flowing through the coils of the electromagnets. Also, the electromagnets are comprised of extendable cylindrical soft magnetic cores that concentrate and enhance the magnetic field strength and gradients along their centres, thus enabling fast catheter tip navigation within the central 3D workspace. Particularly, the soft magnetic material was chosen because of its ability to (i) easily magnetise with the application of an external magnetic field and (ii) quickly demagnetise as soon as the electromagnet currents are switched off. The maximum magnetic field (up to 0.15T) generated by the 8 electromagnets was sufficient to exert the necessary torques and forces on the magnetic-tipped catheter in order to accurately position the tip to a desired target.

The catheter used in the experiments had three seed magnets as illustrated in Fig. 3.1b [55]. The accuracy and efficiency of the quadripolar 3-magnet tip in reaching the desired targets has been demonstrated by two sets of experiments, which were about catheter deflection compared to model-based predictions and verifying the catheter navigation within a heart phantom [46]. According to the results of previous experiments on patient groups [5], the quadripolar 3-magnet tip obtained the highest percentage of successful ablation compared with the 1-magnet tip or bipolar 3-magnet tip. These cases confirm the importance of the optimal design solutions for magnetic-tipped catheters. It is important to note that the seed magnets of the catheter should be appropriately spaced in order to optimise the flexibility of the catheter tip [7].

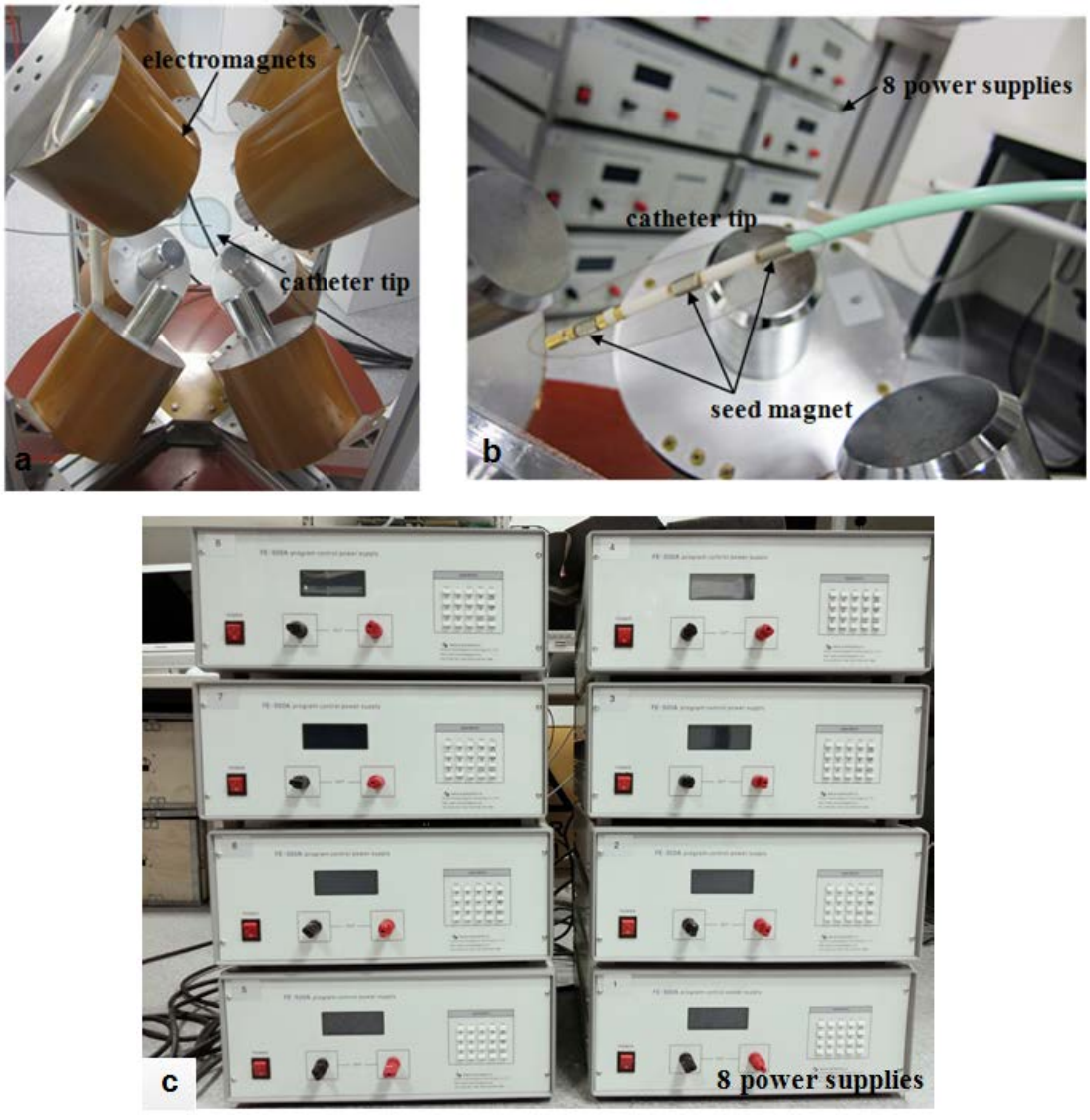

Fig. 3.1. (a) Photograph of the developed magnetic catheter tip positioning electromagnet system demonstrator. (b) Illustration of the catheter tip and its three seed magnets. (c) Eight power supplies.

The designed system comprises eight electromagnets. Each electromagnet has a coil (18 layers, 90 turns per layer, 1.8mm wire diameter, and 4.10Ω±0.05Ω resistance) and a core (made of DT4E pure iron), and is mounted on a hard aluminium frame, after being accurately aligned with respect to the other electromagnets. Each electromagnet coil has an inner diameter d_{inner} =68mm, an outer diameter d_{outer} =140mm, and a length L_{coil} =170mm, and is completely filled with an extractable core made of DT4E pure iron of diameter d_{core} = 66mm and length L_{core} = 279.31mm. These iron cores produce a concentrated magnetic field in the central spherical workspace in order to steer the catheter tip accurately and quickly. The structure of the soft-magnetic-core electromagnet and the dimensions of its components are given in Fig. 3.2.

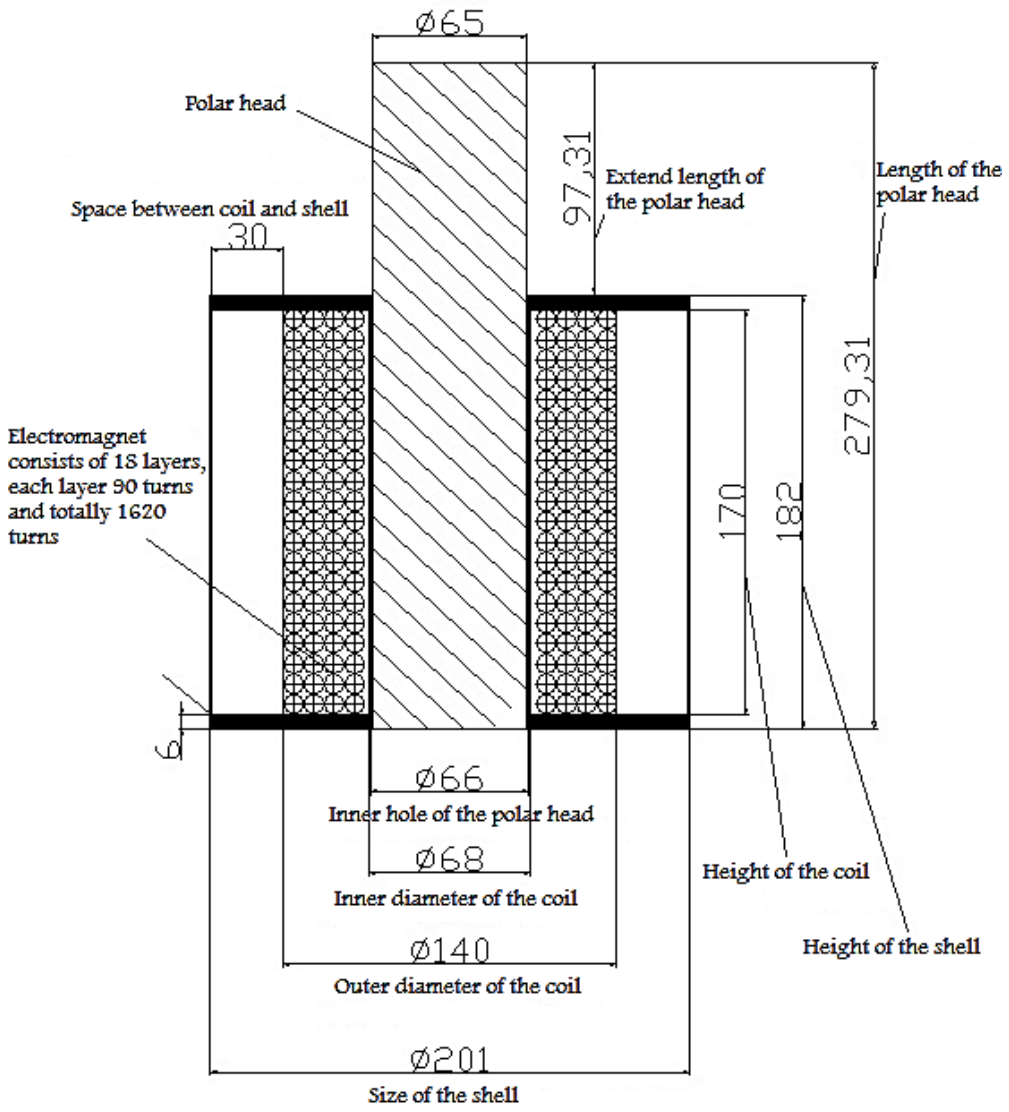

Fig. 3.2. Structure of each electromagnet showing the dimensions of its components

Eight computer-controlled DC power supplies were specifically developed to provide the necessary electric currents to create the desired magnetic field distribution throughout the central 3D workspace. These power supplies are controlled directly through a power supply board that converts AC input of 240V±20V/10A, 50Hz, into a DC output of ±50V/10A. The entire system is controlled through an application written in the language C# and running on a computer Windows 7.0 Operation System. An RS-232 interface is used to control interface with the power supplies for control purposes.

3.2 The total magnetic field of eight iron-core electromagnets

In this system, each electromagnet has many turns and layers wrapped around the extractable iron core as described above. Due to the geometrically complex structures and inhomogeneous materials, it is difficult to compute the applied magnetic field directly. An accurate, effective and versatile numerical computation technique that can be applied to solve this issue is the Finite Element Method (FEM). This method involves subdividing the workspace region of the external magnetic field into a mesh of elements [73-75]. Moreover, these elements can be understood as small magnetic regions around any point P produced by dividing each coil and iron core into many small segments and pieces respectively. To be more obviously, the sections below will present a mathematical model for computing and simulating the total magnetic field of the eight electromagnets by using MATLAB programming.

3.2.1 The total magnetic field of eight coils

As described in Section 3.1, each electromagnet consists of a coil and an extractable iron cores. Consequently, the total magnetic field generated from the electromagnets is computed as the summation of the magnetic field of coils and cores. As pointed out in the Chapter 2, the magnetic field of the current loop is evaluated. In this section, the analysis and calculation of the total magnetic field generated by the eight-electromagnet system is based on the Biot-Savart law [52]. In particular, the mathematical model calculates the total magnetic field of eight coils and cores at any given point P in the central 3D workspace. The total magnetic field generated by a coil is first calculated at a point $P(x_P, y_P, z_P)$ by considering a current element of length dl at a point $C(x_C, y_C, z_C)$ along the coil, as illustrated in Fig. 2.17. The coordinates of C, $\vec{r}(\overrightarrow{CP})$, and $\overrightarrow{dl}$ can be written as

$$\begin{gathered}(x_C, y_C, z_C)_{(R_i, z_j, \theta_k)} = (R_i \cos(\theta_k), R_i \sin(\theta_k), z_j) \\ \vec{r}_{(R_i, z_j, \theta_k)} = \left(x_P - R_i \cos(\theta_k), y_P - R_i \sin(\theta_k), z_P - z_j\right) \\ \overrightarrow{dl}_{(R_i, \theta_k)} = \left(L_i \cos\left(\theta_k + \frac{\pi}{2}\right), L_i \sin\left(\theta_k + \frac{\pi}{2}\right), 0\right) \text{ with } L_i = \frac{2\pi R_i}{Ns}\end{gathered} \tag{14}$$

where R and z denote the radius of the current loop and width of each coil turn respectively, L is the length of each divided current element, i, j and k are the increments for the number of layers, turns and current elements, respectively.

From the Eq. (8), a schematized mathematical formula is presented for calculating the total magnetic field of eight coils in this magnetic catheter steering system. As explained earlier, the principle of superposition is still valid for computing the total magnetic field $\vec{B}_{Coil\,n}$. In other words, the total magnetic field produced by the n[th] coil is expressed as follows:

$$\vec{B}_{Coil\,n} = \frac{\mu_0 I}{4\pi} \sum_{i=1}^{Nl} \sum_{\mathrm{j}=1}^{\mathrm{Nt}} \sum_{k=1}^{Ns} \frac{\overrightarrow{dl}_{(R_i,\theta_k)} \times \vec{r}_{(R_i,z_j,\theta_k)}}{r^3_{(R_i,z_j,\theta_k)}} \tag{15}$$

where Nl, Nt and Ns are defined as the number of layers, turns, and current elements dl respectively. As can be observed in Fig. 3.3, $[C1, \ldots, C8]$ denotes the order of electromagnets from the first to the eighth electromagnets.

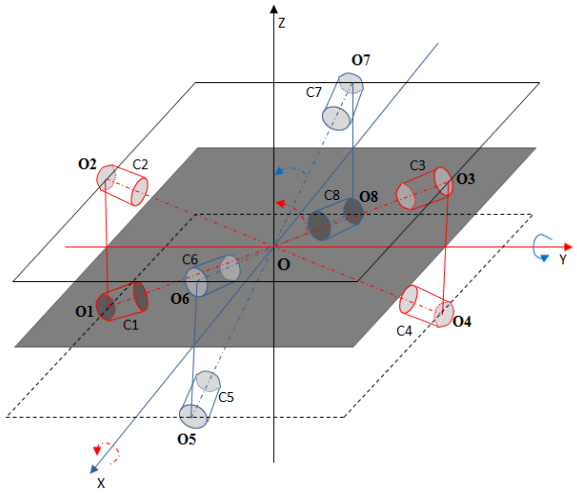

Fig. 3.3. Electromagnet arrangement in 3D. The homogenous transformation of the local coordinate system of each electromagnet is implemented with respect to the global coordinate system Oxyz in the central workspace, in order to sum the magnetic fields generated by the individual electromagnets.

3.2.2 The total magnetic field of eight iron cores

In order to increase the magnetic field strength, each extractable iron core is inserted into eight electromagnets. Specifically, when an electric current flows through the electromagnet, the iron core is magnetized, and the field of the magnetized material adds to the field produced by the wire. Thus, an iron-core electromagnet can produce a magnetic field that is approximately 20 times stronger than that generated by air-

core electromagnets [11]. Furthermore, soft magnetic material is chosen, because it has the advantage that it loses magnetism as soon as the system is switched off.

In order to accurately evaluate the magnetic field, the iron cores were partitioned into small magnetic dipole elements, each of volume dV and magnetic moment dm, as shown in Fig. 3.4 [73, 76]. In addition, each soft magnetic core can be considered as a continuous distribution of dipoles with a magnetic dipole moment $d\vec{m} = \vec{M}dV$ where M is the magnetization vector of the iron core.

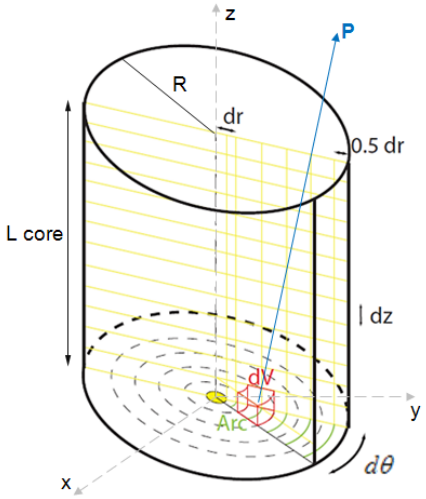

Fig. 3.4. Diagram showing the partitioning of the iron core of an electromagnet for calculating the external magnetic field at a point P in 3D space

MATLAB® was used to compute the external field of each core with the input variables being the number of rounds in the vertical direction (dr is the spacing between turns), the mesh sizes along the horizontal direction (dz) and angular direction ($d\theta$). In other words, the core is divided into many small pieces and arc length of pieces can be supposed as a straight section. Consequently, we can consider the red pieces as rectangular prisms in Fig. 3.4. Furthermore, the individual field contributions produced by each core at any point P in the 3D workspace can be considered as point-dipole interaction model [11]. Thus, the magnetic field of each divided dipole in the iron core is generally calculated as follows [77]:

$$\vec{B}(d\vec{m}, \vec{P}) = \frac{\mu_0}{4\pi}\left(\frac{3\vec{P}(\vec{P}.d\vec{m}) - d\vec{m}}{\|\vec{P}\|^3}\right) \quad (16)$$

where $\mu_0$is the vacuum magnetic susceptibility, $\vec{P}$(m) is the vector with the direction from each dipole to the point P as shown in Fig. 3.4 and $d\vec{m}$ (A.m^2) is the magnetic

moment or the magnetic point-dipole. Overall, the magnetic field and gradient produced at any point P within the workspace is the summation of the magnetic fields generated by the individual point-dipoles of volume dV. Generally, the total magnetic field of the entire core is calculated by developing from Eq.(16):

$$\vec{B}_{core}(\vec{m},\vec{P}) = \frac{\mu_0 M}{4\pi} \sum_{i=1}^{Ndz} \sum_{\mathrm{j}=1}^{\mathrm{Ndr}} \sum_{k=1}^{Nd\theta} \frac{3\,\vec{P}_{ijk}(\vec{P}_{ijk}.\vec{m}_c) - \vec{m}_c}{\left\|\vec{P}_{ijk}\right\|^3} dV_{ijk} \tag{17}$$

where $\vec{m}_c$ (A.m^2) is unitary magnetic moment vector of iron core element, $\vec{P}_{ijk}$ denotes the distance vector from iron core elements to the point P and dV_{ijk} is the volume of core elements.

It can be assumed that if the eight cores are made from an ideal soft-magnetic material with the negligible hysteresis and the cores operate in their linear magnetization region, the field contributions of individual electric currents and gradients can be superimposed linearly. Therefore, if the field contribution of a given electromagnet is precomputed in the workspace, the total magnetic field at any point P in the 3D workspace can be considered as the sum of the contributions of the individual currents as follows [11, 27, 77]:

$$\vec{B}(\vec{P}) = \sum_{e=1}^{n} \vec{B}_e(\vec{P}) = \sum_{e=1}^{n} \tilde{\vec{B}}_e(\vec{P})\, i_e = \mathrm{B}(\vec{P})I \tag{18}$$

where $e = [1,n]$ denotes the e$^{\text{th}}$ electromagnet, i_{en} is the current flowing through the e$^{\text{th}}$ electromagnet, $\tilde{\vec{B}}_e(\vec{P})$ is the unitary current field, $\mathrm{B}(\vec{P}) = \left[\tilde{\vec{B}}_1(\vec{P}) \ldots\ldots \tilde{\vec{B}}_n(\vec{P})\right]$ is a 3xn field matrix at any point P and $I = [i_1 \ldots . i_n]^T$ is a 1xn current matrix.

3.2.3 Transformations in homogeneous coordinates

As the magnetic field vectors have their own direction and magnitude, this point raises the question about summing the field vectors of eight electromagnets with different directions. This section will seek to answer in this question. To sum the individual fields generated by each electromagnet, it is important to transform the local coordinate systems of the eight electromagnets to a global coordinate system Oxyz as shown in Fig. 3.3. As each electromagnet has its own local coordinate system, the coordinates of the vector fields as well as the coordinates of current

segments of electromagnets need to be converted to this global coordinate system. The total of the external magnetic field at the central workspace is calculated by dividing the central space into a grid of points whose coordinates are represented with respect to the reference coordinate system Oxyz.

According to [11, 78], the homogenous transformation matrices from the local coordinate system of each electromagnet to the global coordinate system of the eight-electromagnet system Oxyz can be generally written as:

$$L^O = R_{Cn}^O * T_{Cn}^O * L^{Cn} \quad (19)$$

Eq. (19) is the composition of two transformations, the local coordinate system of eight electromagnets relative to the global coordinate system Oxyz according to the translation T_{Cn}^O and rotation R_{Cn}^O. Moreover, L^{Cn} denotes the matrices of a set of vectors that represent the local coordinates of the electric current elements and core elements in the Cn^{th} electromagnet, where each column of these matrices consists of the components of the corresponding vector of the set. Similarly, L^O denotes the matrices of a set of vectors that represent the global coordinates of the electric current elements and core elements according to the translation and rotation transformations. As presented in Fig. 3.3, the local coordinates from O1 to O8 of the eight electromagnets are translated to the global coordinate O. The coordinate systems of the four electromagnets C1, C2, C3 and C4 are then rotated around the x-axis in an anticlockwise direction with angles $\frac{\pi}{4}, \frac{3\pi}{4}, \frac{5\pi}{4}, \frac{7\pi}{4}$ respectively. Similarly, the coordinate systems of four electromagnets C5, C6, C7, and C8 are rotated around the y-axis in an anticlockwise direction with angles $\frac{\pi}{4}, \frac{3\pi}{4}, \frac{5\pi}{4}, \frac{7\pi}{4}$ respectively. Finally, all local coordinate systems of the eight electromagnets obtain the homogeneous transformations to the global coordinate system. This allows the summation of all the individual magnet field vectors to create the total magnetic field in the 3D workspace.

3.2.4 A flowchart for calculating the external magnetic field of an electromagnet

Fig. 3.5 is a flowchart indicates how to compute the externally generated magnetic field of an electromagnet. As mentioned in the Section 3.1, each electromagnet consists of two parts: coil and core. Hence, coil parameters include radius of coil

(R_coil), number of turns (N_turn) and number of layers (N_layers). Regarding core parameters, it consists of the radius of the iron core (R_dip), core length (L_dip), number of slices (N_dz) and number of rounds (N_dr). These parameters are input in the MATLAB® program to compute the magnetic field of the electromagnet.

Firstly, the electromagnet is divided into elements with each element having an angle `dtheta` angle as depicted in Fig. 2.17. Each angular element is represented by `dtheta = 360/N_dtheta` where `N_dtheta` is the total number of divided angles. On the subsequent step, the coordinate of coil is computed by making a loop process to calculate the coordinate of all elements of the coil from the number of turns `N_turn` to the number of layers `N_layer`. After the loop of coil is completely finished, the program starts to make an iterative process to calculate the coordinate of core. In more detail, the iron core is divided into many pieces and the volume of each piece can be computed as `Arcs = sind (dtheta).*rads` and `ddV = dz*dr.*Arcs` with the average value of two sections `Arcs` and the volume of rectangular prisms `ddV` as described in Appendix B. Next, the calculation of the coordinate of each piece from the number of rounds `N_dr` to the number of slices `N_dz` is repeated. Homogeneous transformation method is applied to transfer all local coordinates of coil and core to the global coordinate system in order that the external magnetic field B can be summed. The final step in the flowchart is to sum the externally applied magnetic field of all elements of the coil and core so that the field strength at any point in the 3D workspace can be determined. For completion, the MATLAB® scripts of this flowchart are listed in Appendix B.

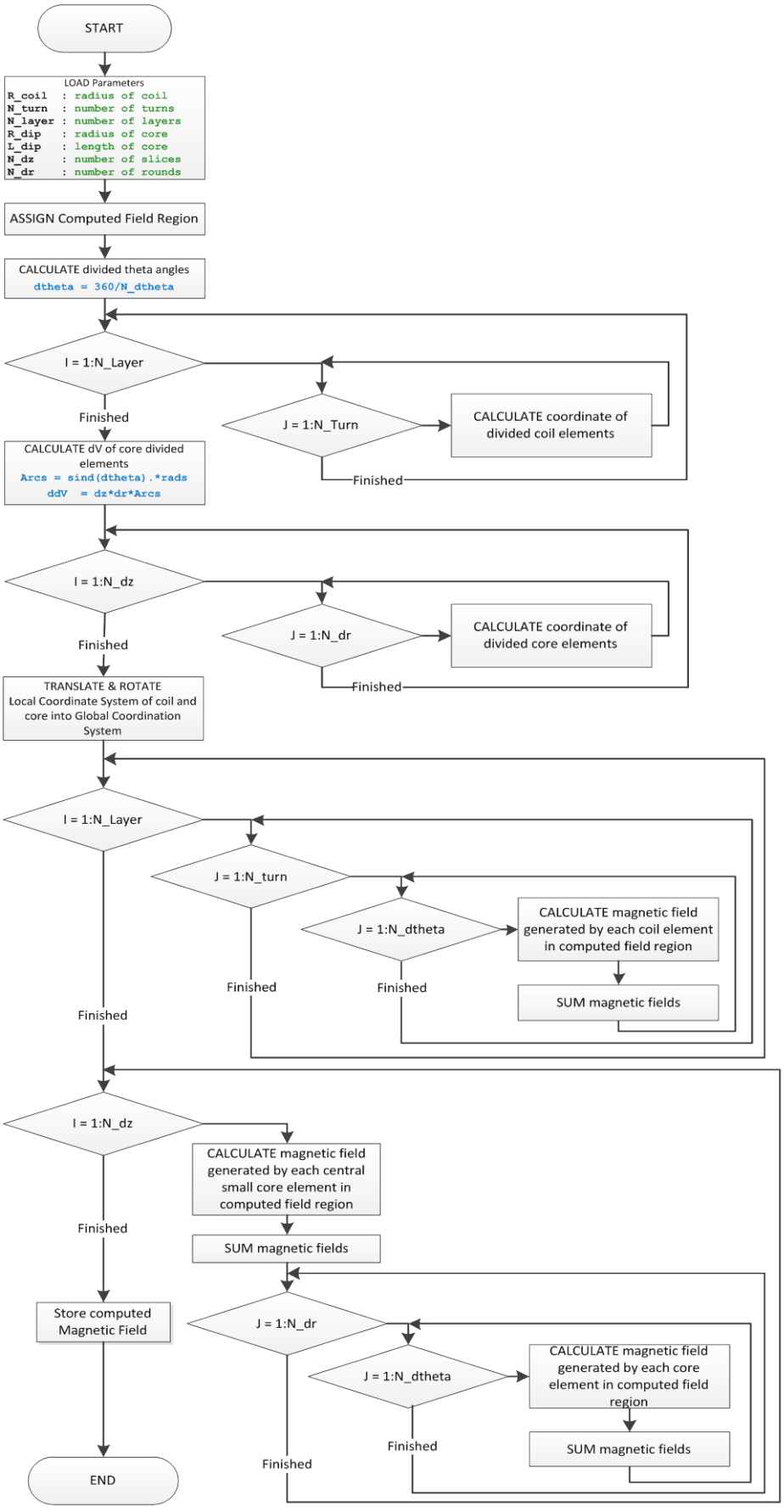

Fig. 3.5. A flowchart to calculate the applied magnetic field of each electromagnet

3.3 Simulation results

The distance between the ends of the two opposite electromagnets for the catheter tip positioning system shown in Fig. 3.1 is 250mm. For simulation, the 128mm×128mm×128mm central 3D workspace is partitioned into eight regions, 0mm is the central position O and 120mm is near the polar head as shown in Fig. 3.6.

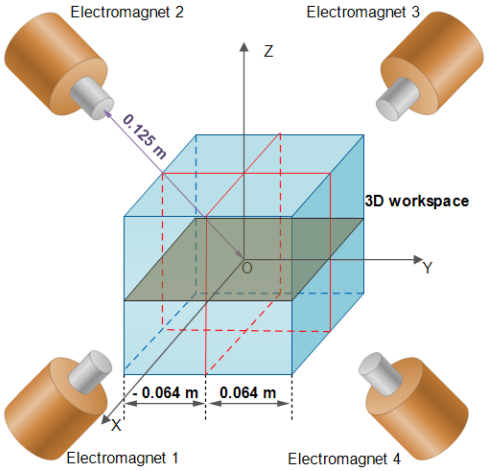

Fig. 3.6. 3D modelling workspace of the remote catheter tip positioning system

The solution of the mathematical model is implemented in MATLAB® with simulated distributions of the magnetic field in the planes xOy, yOz, and xOz, for equal electromagnet currents of 10A presented in Fig. 3.7(b-d). The colour bars symbolize the magnitude of the magnetic field strength. From the measured magnetic field of electromagnets in Appendix A, it is obvious that the magnetic field is strongest at the cores and decreases towards the centre, O, of the workspace. At distances 0mm, 20mm, 40mm, 60mm, 80mm, 100mm and 120mm between the centre O and the core of electromagnet 1, for example, the magnetic field strengths are 0.012T, 0.017T, 0.0244T, 0.0366T, 0.0595T, 0.1003T and 0.136T respectively. It is important to note that the simulation results of the applied magnetic field based on the Eq. (18) is the summation of the magnetic field of coils and extendable cores at any points P in the 3D workspace.

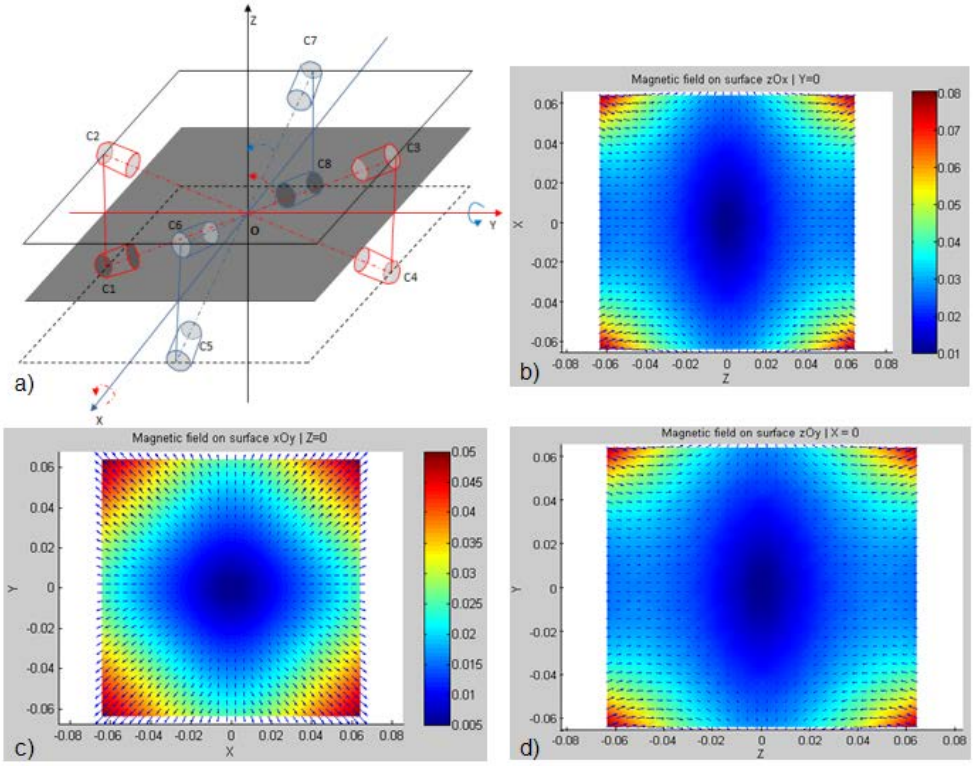

Fig. 3.7. (a) Electromagnets and the reference plane xOy (in grey colour). (b), (c), and (d) Simulated distribution of the total magnetic field generated by the eight electromagnets (driven by equal currents) in planes xOy, yOz and xOz, respectively.

3.4 Simulink model of externally applied magnetic fields

MATLAB's Simulink package was used to investigate perturbations in the magnetic field when the electromagnet current intensities are varied. The block diagrams shown in Fig. 3.8(a) and Fig. 3.9(a) illustrate the simulation procedure followed to vary the electromagnet currents and plot the resultant magnetic field distributions. The simulation procedure comprises (i) *Field_sfcn* block that computes the magnetic field for given input current values based on the mathematical model discussed above and (ii) *Field_dis* block that displays the magnetic field distributions. Both blocks are built at Level-2 MATLAB's s-function.

In the simulation case illustrated by Fig. 3.8(a), it was assumed that the currents driving the eight electromagnets had equal magnitudes, of 10A. The simulated magnetic field distribution, Fig. 3.8(b), exhibits symmetry in planes xOy, yOz and xOz with zero magnetic field at the central coordinate of the system O. In this case,

when the catheter tip is put into the workspace of this system, it is almost at equilibrium.

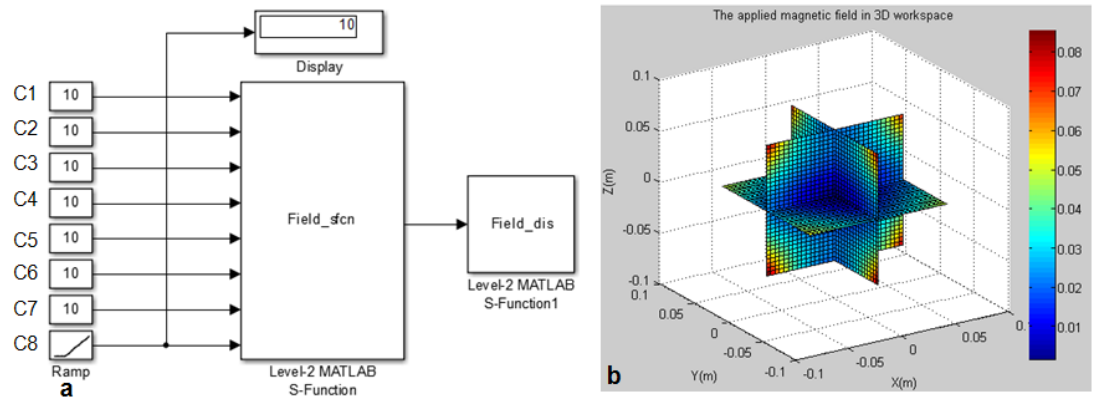

Fig. 3.8. (a) Simulink block diagram illustrating the simulation procedure adopted for varying the electromagnet currents and displaying the magnetic field distribution. (b) Simulated total magnetic field distribution in the 3D workspace for similar electromagnet currents.

Now, let us investigate the effect of changing the electromagnet current values on the magnetic field distribution. Fig. 3.9(a) shows the Simulink block diagram for a scenario where the electromagnet currents were changed to 0A for electromagnets C1, C2, C3 and C4, 10A for electromagnets C5 and C8 and 6A for electromagnets C6 and C7. The simulated magnetic field distribution, shown Fig. 3.9(b), reveals that, in this case, the magnetic field is highest around electromagnets 5 and 8. Therefore, if the catheter tip were placed in the centre of the workspace, it would move upward to a new equilibrium position. Fig. 3.9(c) and (d) show the magnetic field vector distributions in the zOx and zOy planes, which are useful for calculating the forces and torques exerted on the catheter tip.

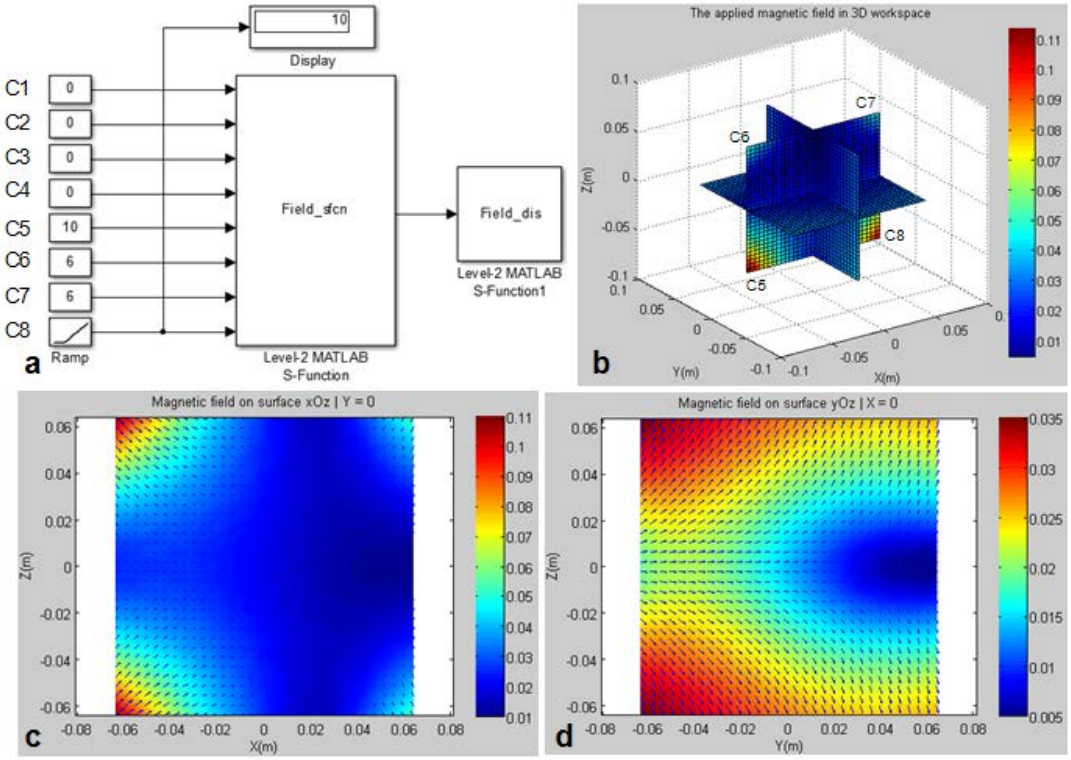

Fig. 3.9. (a) Simulink block diagram for electromagnet current matrix [0 0 0 0 10 6 6 10] Amps. (b) Simulated total magnetic field distribution in the 3D workspace. (c) and (d) Magnetic field vector distributions in the zOx and zOy planes, respectively.

CHAPTER 4 MODELLING TORQUES AND FORCES ACTING ON A CATHETER TIP

To accurately control the catheter tip, the model needs to include the force. Many force models have been developed for precisely positioning magnetic catheters within the heart using externally applied magnetic fields [15, 19]. Three scenarios of forces that act on the flexible portions of the catheter are listed as follows [25]:

- Forces exerted on the magnetic tip of the catheter by externally generated magnetic fields.
- Forces applied along the catheter body when its proximal end is pushed, pulled or twisted.
- Forces arising from the environment such as free space or fluids (flowing blood in the vascular system), gravity and friction. These forces partially affect the catheter tip and body. In a vascular system, the motion of the catheter along flowing blood generates a propulsive force which aids the catheter displacement.

In this chapter, a comprehensive mathematical model for the displacement and deflection of the magnetically-tipped catheter is developed in free space and the tip is affected by magnetic torques, forces and gravitational forces acting on the three magnetic seeds. Future work will develop this model for a fluidic environment.

4.1 Analytical calculation of magnetic torques and forces acting on the three-magnet tip catheter

Villani developed a model that predicts the forces between two magnetic dipoles and validated the model using two methods, (i) vector differentiation and (ii) path integration [79]. For two magnetic dipoles of magnetic moments $\vec{m}_1$ and $\vec{m}_2$, Villani's model expresses the force exerted on the first magnetic dipole due to the second dipole moment as:

$$\vec{F}_{12} = \frac{3\mu_0}{4\pi r^5}\left(\vec{m}_1(\vec{r}.\vec{m}_2) + \vec{m}_2(\vec{r}.\vec{m}_1) + \vec{r}(\vec{m}_1.\vec{m}_2) - \frac{5\vec{r}(\vec{r}.\vec{m}_1)(\vec{r}.\vec{m}_2)}{r^2}\right) \quad (20)$$

where $\mu_0 = 4\pi \times 10^{-7}$ T.m/A is the permeability of free space, $\vec{r}$ is the vector from the central point of the first magnet to the central point of the second magnet and $\hat{r} = \frac{\vec{r}}{|r|}$ is the unit vector parallel to $\vec{r}$.

The force between two magnetic dipoles has been solved [61, 79]. The following analysis develops a comprehensive mathematical model for the magnetic interaction among three-seed magnets and the position and deflection of the catheter tip, when the tip is placed in the 3D external magnetic field. It is important to note that the permanent magnetic seeds inserted into the long rubber tube of catheter are stiff, so they cannot be bent. Consequently, the push and pull components of force $\vec{F}_{pp12}$ and $\vec{F}_{pp21}$ paralleling to $\vec{r}$ can be cancelled out. However, the components of force $\vec{F}_{pe12}$ perpendicular to $\vec{r}$ create a bending moment M_{12} on the catheter tip as shown in Fig. 4.1 [61]. Let $(\widehat{a,b})$ denote the angle between two vectors $\vec{a}$ and $\vec{b}$. The length of the rubber tube between two magnetic seeds is typically small, thus it is accurate to assume that the angle between $\vec{r}$ and $\vec{m}_1$ is approximately zero. As a result, the magnetic interaction force between two dipoles as expressed in Eq. (21) can be rewritten as:

$$\begin{aligned}\vec{F}_{pe12} &= \frac{3\mu_0}{4\pi r^4}\left((m_1\cos(\widehat{\vec{m}_1,\vec{r}})\,.\,m_2\sin(\widehat{\vec{m}_2,\vec{r}}) - m_2\cos(\widehat{\vec{m}_2,\vec{r}})\,.\,m_1\sin(\widehat{\vec{m}_1,\vec{r}})\right) \\ &= \frac{3\mu_0 m_1 m_2}{4\pi r^4}\sin(\widehat{\vec{m}_2,\vec{r}})\end{aligned} \tag{21}$$

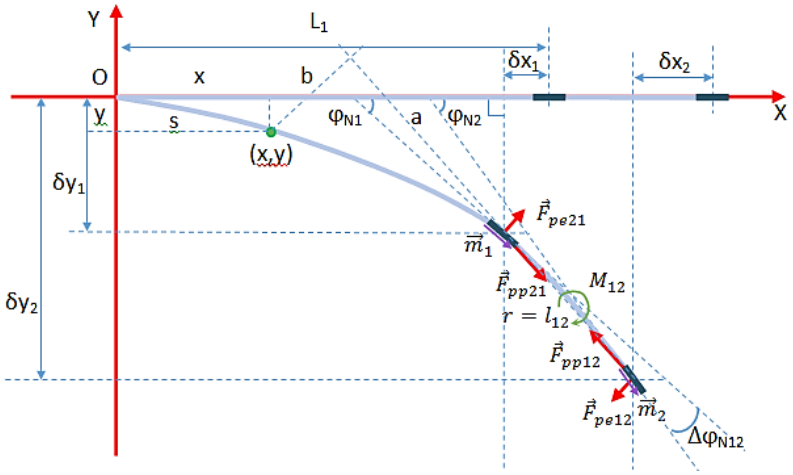

Fig. 4.1. Magnetic forces exerted on two seed magnets attached to the distal tip of the magnetic catheter.

As can be seen from Fig. 4.1, the magnetic interaction between two seed magnets induces a bending moment M_{12} given by

$$M_{12}(s) = F_{pp21}b - F_{pp12}b - F_{pe21}a + F_{pe12}(l_{12}+a) \tag{22}$$

Thus,

$$M_{12}(s) = F_{pe} l_{12} \text{ since } F_{pe21} = F_{pe12} = F_{pe}, \text{ and } F_{pp21} = F_{pp12} \quad (23)$$

Using Eqs. (21) and (23), for a 3-magnet-seed catheter, the bending moment M_{12} exerted on the magnet seeds is:

$$M_{12} = \frac{3\mu_0 m^2}{4\pi l_{12}^3} \sin(\Delta\varphi_{N12}) \text{ with } \Delta\varphi_{N12} = \varphi_{N1} - \varphi_{N2} \quad (24)$$

Similarly, the bending moments M_{23} and M_{13} can be expressed as:

$$M_{23} = \frac{3\mu_0 m^2}{4\pi l_{23}^3} \sin(\Delta\varphi_{N23}) \text{ with } \Delta\varphi_{N23} = \varphi_{N2} - \varphi_{N3} \quad (25)$$

$$M_{13} = \frac{3\mu_0 m^2}{4\pi l_{13}^3} \sin(\Delta\varphi_{N13}) \text{ with } \Delta\varphi_{N13} = \varphi_{N1} - \varphi_{N3} \quad (26)$$

where $\varphi_{Nm}, m = 1,2,3,$ is the angle between the x-axis and the dipole moment vector of m^{th} magnetic seed. Note that the bending moments depend on the angles $\Delta\varphi_{N12}, \Delta\varphi_{N23}, \Delta\varphi_{N13}$ and the separation distances, l_{12}, l_{23}, l_{13}, between the magnetic seeds.

The dimensions of the catheter tip used in this mathematical model were taken from the specifications of the irrigated gold tip catheter Trignum Flux G, made by Biotronik, Germany. This catheter was chosen because of its flexibility, safe operation and ablation effectiveness [14, 80]. Each of the three identical cylindrical seed magnets has a length of 6-mm and a diameter of 2.3mm, and the spacing between the first and second seed magnets and the second and third seed magnets are 9.5mm and 15.5mm, respectively, as illustrated in Fig. 4.2. The magnetic seeds are made using an alloy of neodymium-iron-boron (NdFeB), which exhibits a remanent magnetization of approximately 5×10^5 A/m [12, 64, 81]. Particularly, this ferromagnetic material is widely utilized in catheter designs, because it has strong magnetisation, making it an excellent candidate for steering catheter tips [82-84]. The Finite Element Method was applied for the simulation of the curvature of the catheter tip under an external magnetic field, taking into account the magnetic interaction among seed magnets. Note that, in this thesis, the analysis concentrates on the torques and forces exerted on the three magnetic seeds; other factors such as the four electrodes embedded into the catheter tip can be assumed to be neglected, because they have negligible impact on the catheter motion [19].

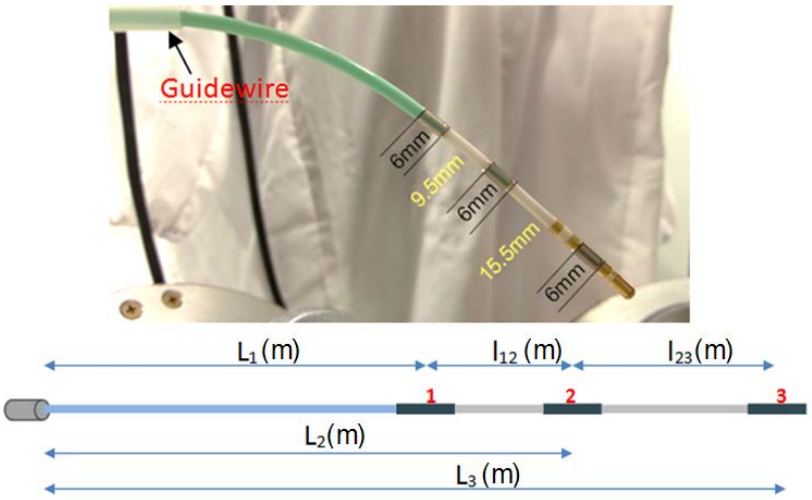

Fig. 4.2. Irrigated gold tip catheter and its dimensions

As reported in Chapter 2, the Euler-Bernoulli beam theory was applied to establish the equilibrium equation of the catheter tip in an external magnetic field. Some parameters needed to be defined, such as the slope at any point C(x,y) with respect to the x-axis, φ, and the arc length from the fixed end of the catheter tip to point C(x,y), s. Furthermore, the bending rigidity of the catheter tip was modelled through two different values, namely, the lengths $L1, l_{12}$ and l_{23}, illustrated in Fig. 4.2. Next, Fig. 4.3(a) illustrates the forces, bending moments and torques typically exerted on the three seed magnets of the catheter. The total forces $\{F_{t1}, F_{t2}, F_{t3}\}$ exerted on three magnets are the sums of the magnetic forces $\{F_{m1}, F_{m2}, F_{m3}\}$ and gravitational forces $\{P_1, P_2, P_3\}$. In order to determine the catheter position, it is necessary to evaluate the horizontal and vertical displacements, $\{\delta_{x1}, \delta_{x2}, \delta_{x3}\}$ and $\{\delta_{y1}, \delta_{y2}, \delta_{y3}\}$, as well as the angles $\{\varphi_{N1}, \varphi_{N2}, \varphi_{N3}\}$, illustrated in Fig. 4.3(a). Note that, the seed magnets inserted into the long rubber tube of catheter are assumed to be stiff, so they cannot be bent as illustrated in Fig. 4.3(b).

Being made of permanent magnetic material, the magnetization M of each magnet seed is therefore independent of the magnetic field generated by the electromagnet system. Furthermore, the magnetization of each magnetic seed depends on the remanent magnetization of NdFeB and the shape of the seed. The torque exerted on a magnet seed depends on the angle between $\vec{M}$ and $\vec{B}$, which can be adjusted incrementally up to 90^o. To increase the force exerted on a magnet seed, the magnetic gradient must be increased through the control of the distribution of the

magnetic field generated by the electromagnet system [27]. Note that in order to accurately model the catheter motion, it is important to take into account not only the magnetic torque induced by the cross products of the applied magnetic field and magnetic moments, but also the torque generated by the cross products of the lever-arm distance and the total forces (including magnetic forces and gravitational forces). In the following section, we derive the equations that simulate the equilibrium state of the catheter tip, based on the analytical solution of torques and forces.

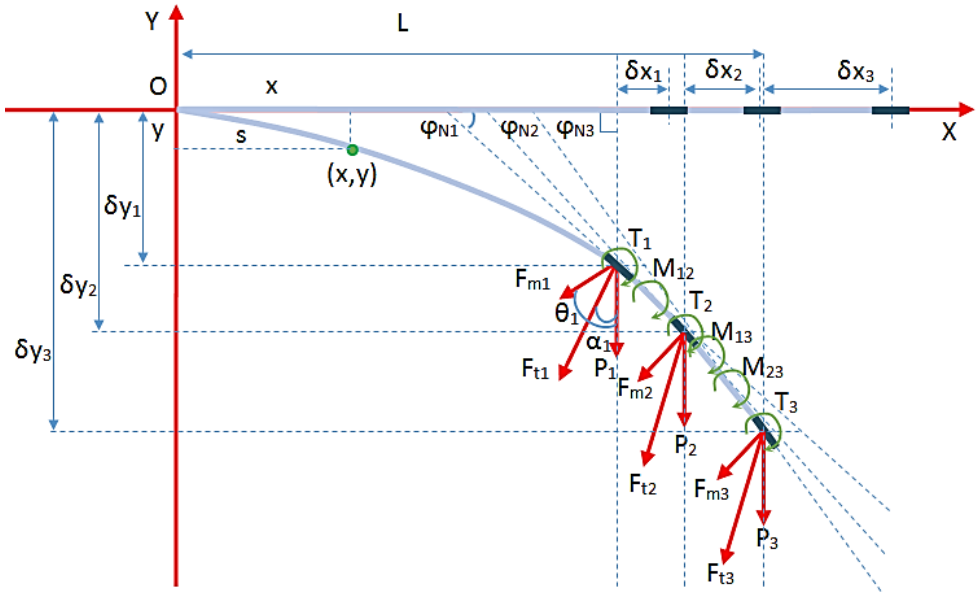

(a)

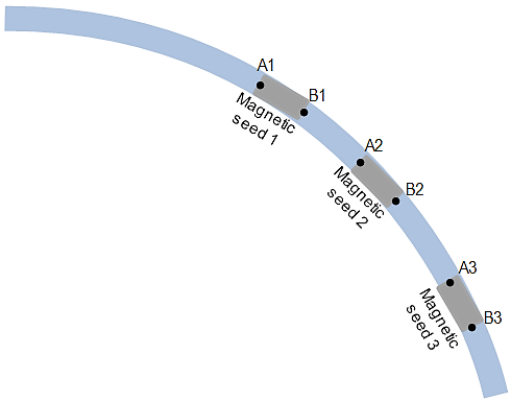

(b)

Fig. 4.3. (a) Illustration of the distribution of forces, bending moments and torques exerted on the three seed magnets of a catheter. (b) Definition of points {Ai, Bi} on the magnet seeds.

4.2 Catheter equilibrium state modelling

As mentioned previously, the catheter is inextensible and has a long thin body with a diameter that is much smaller than its length, as illustrated in Fig. 4.2. As such, the Euler-Bernoulli beam model can be applied to predict the curvature of the catheter [19, 67-70], with the catheter considered to be a cantilever beam that is fixed at one end and free at the other. According to the study of the deflection of the cantilever beam reported by Feynman et al. [68], the Euler-Bernoulli bending moment (M)-curvature (φ) relationship can be expressed as $EI\frac{d\varphi}{ds} = M$, where $\frac{d\varphi}{ds}$ is the curvature

of the catheter at any point along its length, M denotes the bending moment, and EI is bending rigidity of the catheter [37]. By differentiating this equation with respect to the distance s, we obtain [70]:

$$EI\frac{d^2\varphi}{ds^2} = \frac{dM}{ds} \tag{27}$$

The total bending moment can be expressed as the sum of the bending moments acting on the three magnets of the catheter tip, that is:

$$M(s) = \begin{cases} M_1(s) + M_2(s) + M_3(s) + M_0(s), & 0 < s < L_1 \\ M_2(s) + M_3(s) + M_0(s), & L_1 < s < L_2 \\ M_3(s) + M_0(s), & L_2 < s < L_3 \end{cases} \tag{28}$$

Note that, unlike the simplified analysis presented in [70], where the deflection of the beam is caused by one vertical concentrated load at the free end, and the mass of beam is omitted, the weight of catheter tip is taken into account in the modelling. With respect to Fig. 4.3, assuming that the components of the total forces $\{F_{t1}, F_{t2}, F_{t3}\}$ along the x- and y- axes are $\{F_{t1x},\ F_{t2x},\ F_{t3x}\}$ and $\{F_{t1y},\ F_{t2y},\ F_{t3y}\}$, respectively, therefore, the bending moments M_1, M_2, M_3 and M_0 at the three seed magnets and the fixed end of the catheter, respectively, can be expressed as

$$M_1(s) = F_{t1y}(L_1 - \delta_{x1} - x) + F_{t1x}(\delta_{y1} - y) \tag{29}$$

$$M_2(s) = F_{t2y}(L_2 - \delta_{x2} - x) + F_{t2x}(\delta_{y2} - y) \tag{30}$$

$$M_3(s) = F_{t3y}(L_3 - \delta_{x3} - x) + F_{t3x}(\delta_{y3} - y) \tag{31}$$

$$M_0 = \begin{cases} T_1 + T_2 + T_3 + M_{12} + M_{23}, & 0 < s < L_1 \\ T_2 + T_3 + M_{23}, & L_1 \le s < L_2 \\ T_3, & L_2 \le s < L_3 \end{cases} \tag{32}$$

Eq. (32) shows that a moment M_0 applied at the end of the tip is the total of magnetic torques T_1, T_2, T_3 produced by the external magnetic field and the bending moments M_{12}, M_{23}, M_{13} among three magnets. It is essential to note that the spacing between magnetic seeds is intentionally made different in order to make the magnetic interaction between them negligible [61]. As explained above, the applied spacing between magnetic seeds attached to the catheter tip can be assumed to be similar to the designed spacing of the Trignum catheter tip (Biotronik, German) in this scenario.

Differentiating Eq. (29), (30), (31) and (32) with respect to s, and using $\frac{dM_0}{ds} = 0$ (because the components of the bending moment M_0 are independent of the

distance s), $\frac{dx}{ds} = \cos\varphi$ and $\frac{dy}{ds} = \sin\varphi$, the equilibrium equation for the catheter tip can be expressed as follows [70, 85]:

$$EI\frac{d^2\varphi}{ds^2} + F_{t1y}\cos\varphi_n + F_{t1x}\sin\varphi_n + F_{t2y}\cos\varphi_n + F_{t2x}\sin\varphi_n + F_{t3y}\cos\varphi_n + F_{t3x}\sin\varphi_n = 0 \quad (33)$$

$$\Leftrightarrow EI\frac{d^2\varphi}{ds^2} + (F_{t1y} + F_{t2y} + F_{t3y})\cos\varphi_n + (F_{t1x} + F_{t2x} + F_{t3x})\sin\varphi_n = 0 \quad (34)$$

The boundary conditions for this differential equation are written as

$$\varphi|_{s=0} = 0;\ \left.\frac{d\varphi_n}{ds}\right|_{s=0} = 0, \quad (35)$$

$$\frac{d\varphi_N}{ds} = \frac{l_{12}F_{t2y}cos\varphi_N + l_{12}F_{t2x}sin\varphi_N + l_{13}F_{t3y}cos\varphi_N + l_{13}F_{t3x}sin\varphi_N + M_0}{EI} \quad (36)$$

$$\frac{d\varphi_{N2}}{ds} = \frac{l_{23}F_{t3y}cos\varphi_{(N1)} + l_{23}F_{t3x}sin\varphi_{(N1)} + M_0}{EI} \quad (37)$$

$$\frac{d\varphi_{N2}}{ds} = \frac{M_0}{EI} \quad (38)$$

where $d\varphi_n \triangleq \varphi_n - \varphi_{(n-1)}$. In addition, assume that {Ai, Bi} are the points at the front end of the i[th] magnet seed, as shown in Fig. 4.3(b), since the three seed magnets are not flexible materials, they cannot be deformed like the elastic material of the catheter body. In other words, for points within the three seed magnets, the bending constraints of the seed magnets are expressed as follows;

$$\varphi|_{s\in[Ai,Bi]} = constant \quad (39)$$

As mentioned above, the catheter tip can be considered as a cantilever beam. Therefore, analytical solutions to the equilibrium equation of the cantilever beam under the manipulation of the external magnetic field are investigated. In 1961, Wang et al. addressed the second-order differential equation for the deflection of cantilever beam by applying Southwell's relaxation technique [86]. However, when this method was applied in this study, it took a long time for the MATLAB® program to run an iterative procedure in order that the catheter tip could converge on the new equilibrium position. Because this method results in relatively high errors, it is inappropriate to meet the demands for identifying expected targets with high accuracies.

The second order ordinary differential equation in Eq.(33) presents the continuous variation. There have been many solutions to a system of ODEs. Firstly, an Initial Value Problem (IVP) solver has handled the ODE and often has a unique solution.

However, in the case of solving the equilibrium configuration of the three-magnet catheter tip, the boundary conditions are established on three magnetic seeds in a more complex way, because they specify the deflection of the catheter tip at more than one point. Consequently, the Boundary Value Problem (BVP) is more difficult to solve than the IVP and may have none or more than one solution as opposed to the IVP [87]. Due to this, it is very important to provide a suitable guess for the solution desired for solving the BVP, which is often the hardest part of solving the BVP.

To solve Eq. (34) using the boundary value problems and stated boundary conditions, "MATLAB bvp4c solver" is applied in this thesis. According to the built-in boundary value problem solver in MATLAB library, a bvp4c solver is considered as a collocation method that implements the three-point Lobatto IIIA implicit Runge-Kutta formula. According to [88], the Simpson method as well as bvp4c provide a uniform prescribed accuracy throughout the computational interval. Furthermore, an implicated design and algorithm in the bvp4c solver has made the BVP become to be solved easier and taken a remarkable method to the control of error in order to help it cope with poor guesses. This method is started with an initial guess supplied at an initial mesh of points to divide the interval of integration into subintervals. The solver applies a finite difference solution to address the equilibrium equation and boundary conditions. After that, the error of this numerical solution is estimated on each subinterval. If the error does not satisfy the tolerance criteria, the bvp4c solver adjusts the step size, and repeats the process to achieve the specified accuracy [87-89].

4.3 Magnetic catheter guidance model

The guidance of the magnetic catheter is obtained by generating the appropriate external magnetic field that produces the moments necessary for bending the catheter to a desired angle. Due to the computational complexity of the total magnetic field generated by eight electric currents, a unit-current magnetic field map can be pre-computed as mentioned in Eq. (18), for the electromagnetic-based magnetic catheter tip positioning system demonstrator illustrated in Fig. 3.1. The external magnetic field is generated by driving the electromagnets with a set of electric currents, called driving currents and represented by the matrix $\bar{I}$. The magnetic field, forces and torques exerted on the magnet seeds can be calculated using Eqs. (9), (12) and (18).

The magnetic forces and torques, which depend on the spacing, shape and size of the magnetic seeds, induce bending moments that can be calculated using Eq. (27). While the catheter tip and magnet seeds can be moved while the catheter is bending, it is difficult to directly determine the position of the catheter for a given driving current matrix $\bar{I}$, because the magnetic force and torque exerted on the catheter's magnet seeds are not constant when the catheter is being deflected.

An iterative algorithm was especially developed, which executes steps in iterations and successive approximations in order to obtain the catheter's position. The algorithm can be described as follows: The calculation begins with the initial position of the magnetic seeds, then the magnetic forces and torques are computed according to the current position of catheter tip, and then the various bending moments are obtained to predict the new position of the catheter. The calculation of the forces and torques is then repeated with the new position and the process is iterated until the predicted position of catheter tip converges to a stable position that satisfies the boundary conditions. Note that if the distance between the consecutive catheter positions as well as the difference between the consecutive values of the forces and torques are large, convergence may not be practically attainable. To solve this issue, a fast and efficient calculation method is proposed that can be described as follows:

First, instead of conventionally recalculating the magnetic field at the position of the magnetic seeds when the catheter is bent, the magnetic field distribution generated within the 3D workspace by the eight electromagnets with unitary driving electric currents (I_u) is pre-computed and stored as a 3D matrix $B_e = \{B_{e_1}, B_{e_2}, \dots, B_{e_8}\}$. The magnetic field distribution, B_s , around the catheter seeds (for a catheter position s) is then efficiently calculated from B_e, and can be represented by a function $\mathfrak{F}_s$ given by:

$$B_s = \mathfrak{F}_s(I, B_e) \triangleq \sum_{i=1}^{8} \frac{I_i}{I_u} . B_{ei}\,(\mathrm{s}) \tag{40}$$

Secondly, to accelerate the convergence of the iterations to the equilibrium position of the catheter tip we express each driving current flowing through each electromagnet as the product of two parts, namely a primary current, I_P, and a steering factor, A_S, that is

$$\bar{\mathrm{I}} = A_S \, . I_P \tag{41}$$

Using Eqs. (40) and (41) yield

$$B_s = A_S . \mathrm{F}_s(I_P, B_e) \tag{42}$$

The primary current matrix, $I_P = [I_{P_1}, I_{P_2}, \dots, I_{P_8}]$, affects the direction of magnetic field , while the steering factor, A_S, steers the magnetic field direction through small current increments that gradually change the direction and magnitude of the magnetic field to the desired value.

Thirdly, an iterative process is used to determine the equilibrium position of catheter tip, which is illustrated by the flow chart of Fig. 4.4. To begin with, the tip is placed along a defined initial position within the central workspace with zero driving currents. Next, the current values of the eight electromagnets are gradually increased. The distribution of the generated magnetic field is then calculated at every increment of the electric current to evaluate the forces and torques exerted on the catheter and the next stage is to compute the new position and deflection of the catheter tip at every increment of the electric current. The algorithm iterates until the solution for the final equilibrium position of the catheter tip converges. Note that by reducing the current increment, the catheter can be positioned more accurately at a desired destination; however, the drawback is that the convergence time increases. A trade-off therefore exists between the catheter positioning accuracy and required algorithm convergence time.

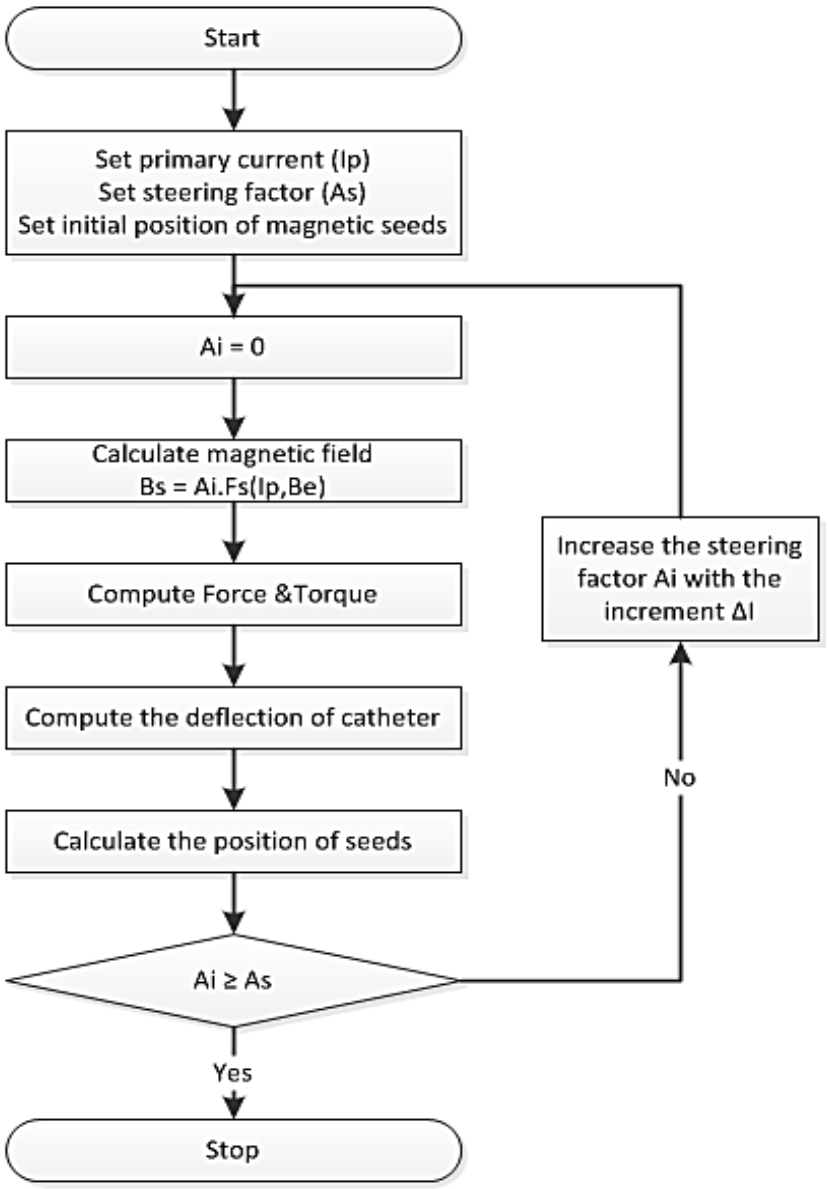

Fig. 4.4. Flowchart illustrating the iterative algorithm used to find a new equilibrium position of the catheter tip in the workspace.

4.4 Simulation and experimental results

4.4.1 Simulation results

In order to determine the current position of the catheter tip in the workspace, it is important to map the local coordinate system of the catheter into the global coordinate system of the eight-electromagnet system. Assuming that the three-magnet tip catheter is placed along the negative direction of the x-axis in the plane xOz, and the guidewire position is at a distance 0.064m from the centre O of the workspace as illustrated in Fig. 4.5(a). The simulated magnetic field distributions

shown in Fig. 4.5(b) present that the deflection of the catheter tip, when the current values of four electromagnets C5, C6, C7, and C8 are progressively increased from 0A to 2A. In addition, the two upper electromagnets are assumed to attract the catheter tip, whereas the two lower electromagnets repel the tip. Note that for all displacements, the magnetic seeds are aligned with the direction of the magnetic field, as illustrated in Fig. 4.5(c). In other words, this system model is verified by the direction of the catheter tip aligned with the direction of the applied magnetic field and the catheter tip is bent upwards as in Fig. 4.5(b). Table 4.1 presents all used parameters of the magnetic seed and catheter used in this model. These parameters can be changed to create a catheter tip with different characteristics such as material, diameter, and bending stiffness, and the model can be used to predict the position of the new catheter tip. This is very flexible and efficient for positioning the different types of catheter tip in the externally applied magnetic field.

Parameter	**Symbol**	**Value**
Bending stiffness	EI (Nm2)	9×10^{-6}
Magnetization	M (A/m)	5×10^{5}
Magnetic seed density	kg/m^3	7500
Diameter of magnetic seed	r (m)	0.0023
Volume of hollow cylindrical seed	V (m^3)	1.923×10^{-8}
Mass of each hollow cylindrical seed	w (kg)	1.44×10^{-4}
Length between the guidewire and 1^{st} seed	L1 (m)	0.040
Length between the 1^{st} and 2^{nd} seed	l12 (m)	0.015
Length between the 2^{nd} and 3^{rd} seed	l23 (m)	0.021

Table 4.1. Parameters representing the properties of the magnetic seeds and catheter used in the simulation model

From the magnitude of magnetic torque and moment of force in Table 4.2, it is apparent that the magnetic torque plays a dominant role in steering the three-magnet tip catheter in the direction of the externally applied magnetic field. When the curvature of the tip is increasing at each electric current value, the magnitudes of magnetic torque and moment of force acting on three magnetic seeds also vary, corresponding to each current increment. Table 4.2 shows values of magnetic torque

and moment of force corresponding to the displacement and deflection of catheter tip as in Fig. 4.5b.

Step size	Magnetic torque			Moment of force		
	1st seed	2nd seed	3rd seed	1st seed	2nd seed	3rd seed
3	-9.73e-06	-9.17e-06	-8.36e-06	1.53e-06	2.04e-06	1.93e-06
4	-2.02e-05	-1.90e-05	-1.74e-05	3.31e-06	3.63e-06	1.94e-06
5	-3.12e-05	-2.90e-05	-2.80e-05	5.34e-06	4.24e-06	6.22e-07
6	-4.24e-05	-3.99e-05	-3.91e-05	7.10e-06	4.77e-06	-1.53e-06
7	-5.36e-05	-5.06e-05	-5.02e-05	9.11e-06	5.33e-06	-3.61e-06
8	-6.41e-05	-6.05e-05	-5.98e-05	1.08e-05	6.27e-06	-4.17e-06
9	-7.39e-05	-6.92e-05	-6.78e-05	1.23e-05	7.06e-06	-3.18e-06
10	-8.27e-05	-7.71e-05	-7.43e-05	1.35e-05	8.86e-06	-5.38e-07
11	-9.04e-05	-8.35e-05	-7.89e-05	1.43e-05	9.62e-06	3.84e-06
12	-9.87e-05	-9.15e-05	-8.41e-05	1.60e-05	1.61e-05	1.16e-05
13	-1.06e-04	-9.82e-05	-8.89e-05	1.68e-05	1.70e-05	1.87e-05
14	-1.13e-04	-1.03e-04	-9.19e-05	1.71e-05	1.74e-05	2.17e-05
15	-1.20e-04	-1.10e-04	-9.76e-05	1.75e-05	1.79e-05	2.53e-05
16	-1.31e-04	-1.19e-04	-1.07e-04	1.79e-05	1.85e-05	2.96e-05

Table 4.2. Magnetic torques and moment of forces for the scenario shown in Fig. 4.5(b)

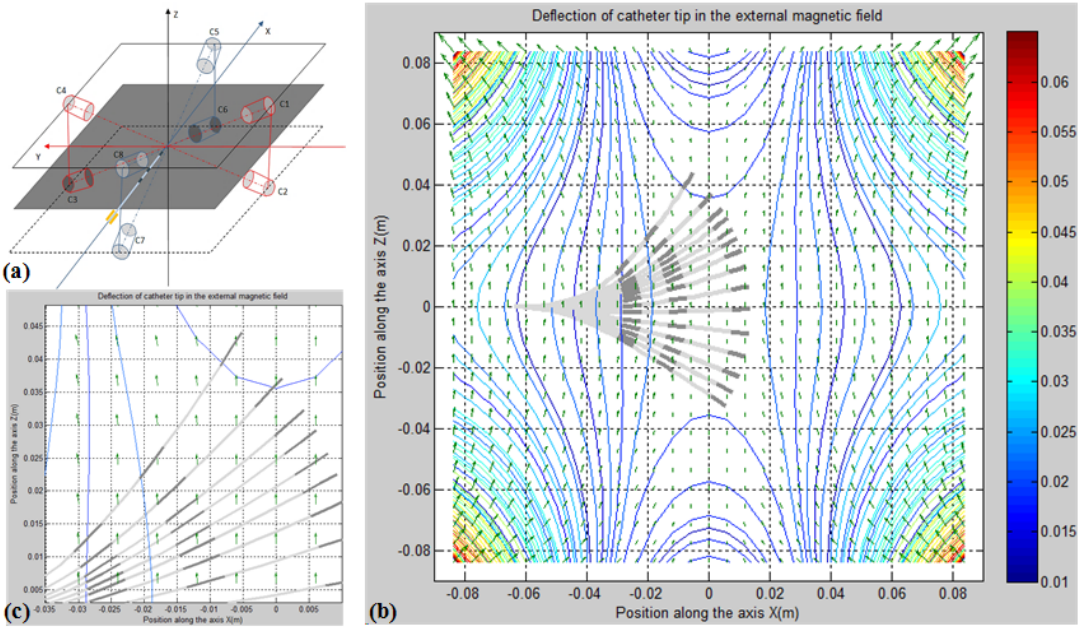

Fig. 4.5. (a) Illustration of the electromagnet system, (b) Simulated catheter tip deflection in the applied magnetic field, and (c) zoom-in of (b).

Similarly, the electric current values of four electromagnets C5, C6, C7, and C8 are progressively increased from 0A to 2A. The two upper electromagnets are assumed to repel the catheter tip, whereas two lower electromagnets are to attract the tip. The simulation result in Fig. 4.6 demonstrates that the direction of the catheter tip is changed based on the repulsion and attraction of electromagnets.

Step size	**Magnetic torque**			**Moment of force**		
	1st seed	**2nd seed**	**3rd seed**	**1st seed**	**2nd seed**	**3rd seed**
3	9.54e-06	8.79e-06	7.78e-06	-1.54e-06	-1.94e-06	-2.85e-06
4	1.84e-05	1.68e-05	1.52e-05	-2.80e-06	-3.63e-06	-6.49e-06
5	2.66e-05	2.41e-05	2.14e-05	-3.84e-06	-5.08e-06	-1.17e-05
6	3.42e-05	3.27e-05	2.70e-05	-4.63e-06	-7.88e-06	-1.54e-05
7	4.11e-05	3.89e-05	3.14e-05	-5.18e-06	-8.85e-06	-2.25e-05
8	4.94e-05	4.45e-05	3.85e-05	-5.25e-06	-9.33e-06	-2.53e-05
9	5.53e-05	4.94e-05	4.24e-05	-5.13e-06	-9.53e-06	-2.78e-05
10	6.07e-05	5.38e-05	4.59e-05	-4.84e-06	-9.45e-06	-2.98e-05
11	6.67e-05	6.08e-05	5.66e-05	-4.54e-06	-1.26e-05	-3.49e-05
12	6.99e-05	6.45e-05	5.49e-05	-3.31e-06	-5.37e-06	-2.99e-05
13	7.37e-05	6.75e-05	5.71e-05	-2.20e-06	-3.35e-06	-2.86e-05
14	7.07e-05	6.27e-05	6.43e-05	1.40e-06	3.26e-06	-1.52e-05
15	7.39e-05	6.49e-05	6.67e-05	2.86e-06	5.90e-06	-1.05e-05
16	7.55e-05	6.57e-05	8.08e-05	5.91e-06	1.13e-05	1.91e-05

Table 4.3. Magnetic torques and moment of forces for the scenario shown in Fig. 4.6(a)

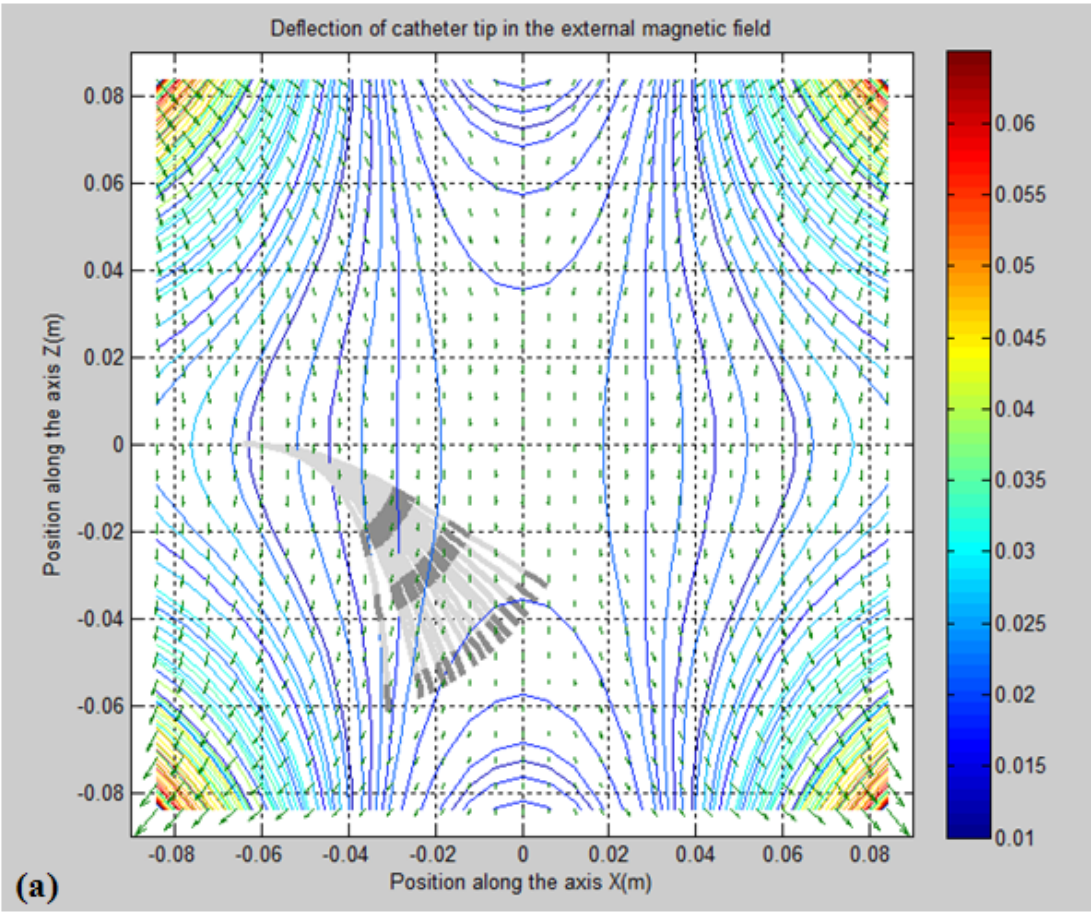
Deflection of catheter tip in the external magnetic field
Position along the axis Z(m)
Position along the axis X(m)
0.08
0.06
0.04
0.02
0
-0.02
-0.04
-0.06
-0.08
0.06
0.055
0.05
0.045
0.04
0.035
0.03
0.025
0.02
0.015
0.01
(a)

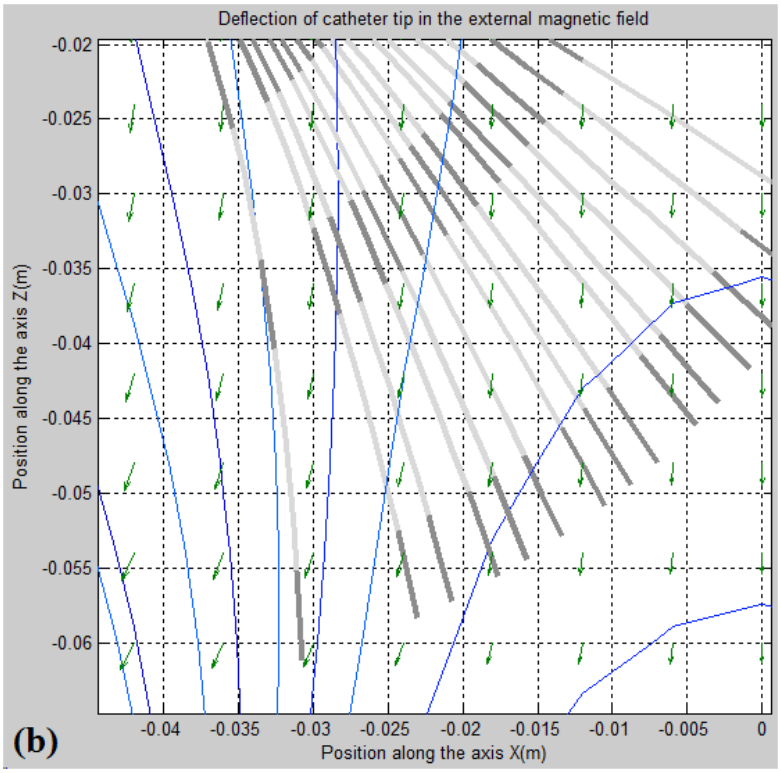
Deflection of catheter tip in the external magnetic field
Position along the axis Z(m)
Position along the axis X(m)
-0.02
-0.025
-0.03
-0.035
-0.04
-0.045
-0.05
-0.055
-0.06
-0.04
-0.035
-0.03
-0.025
-0.02
-0.015
-0.01
-0.005
0
(b)

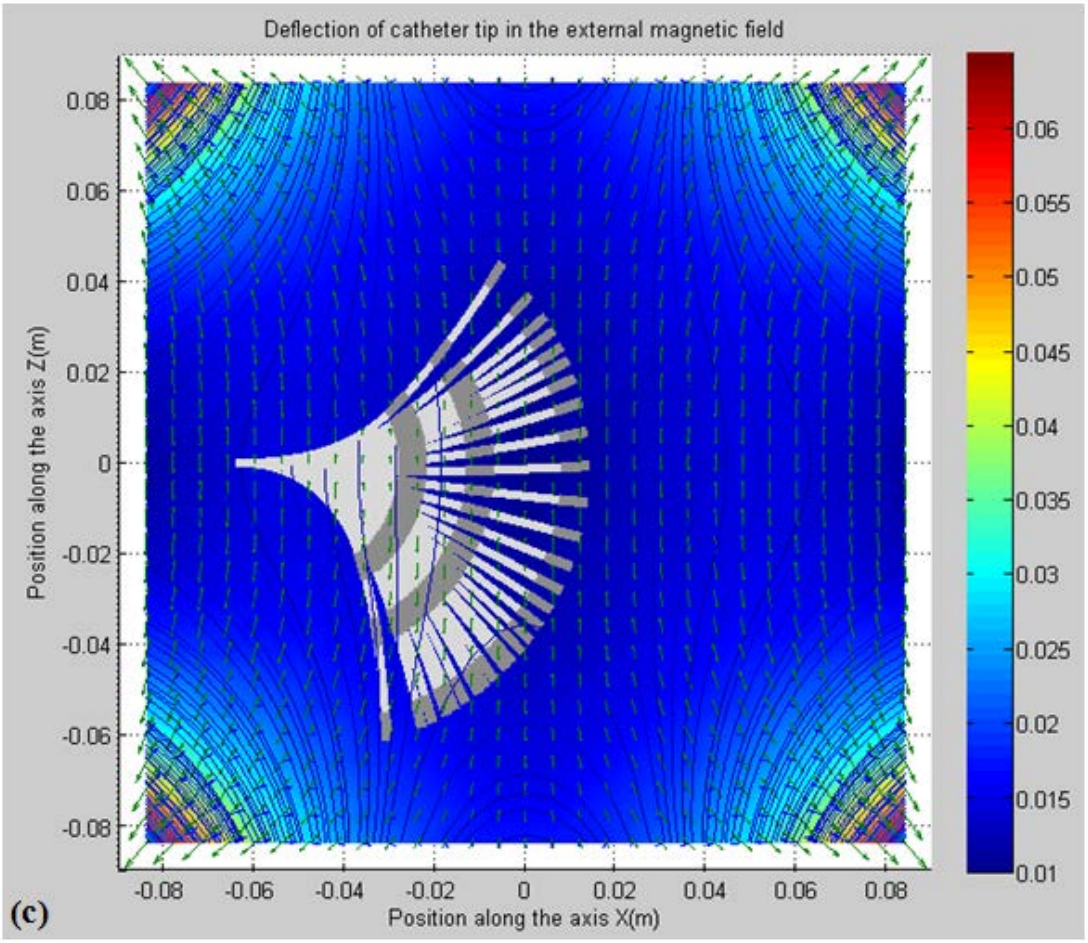

Fig. 4.6. (a) The catheter tip is bent downwards, when the current is steadily increased from 0A to 2A. The two upper electromagnets are assumed to repel the catheter tip, whilst the two lower electromagnets attract the tip. (b) zoom-in of (a). (c) The catheter tip moves upwards and downwards in the externally applied magnetic field.

4.4.2 Experimental setup and results

As described in Chapter 3, Section 3.1, the system software interface was written in the programming C# language. The electric current values are adjusted to 7A using this interface and then click on auto update box as shown in Fig. 4.7, in order to remotely control the catheter tip in the workspace.

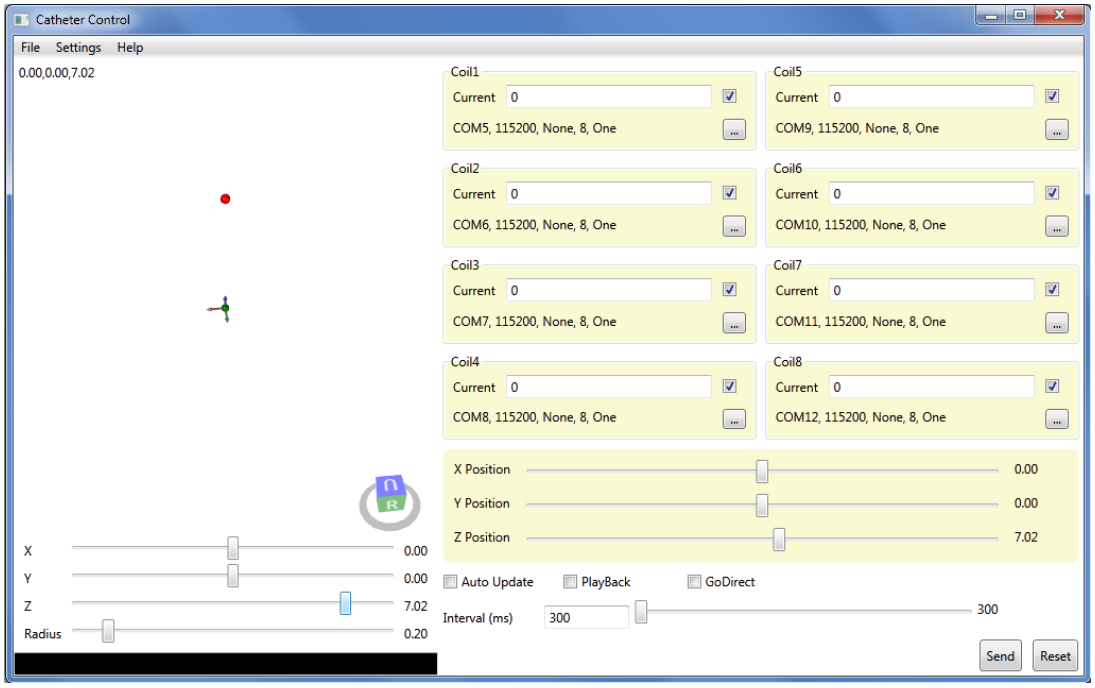

Fig. 4.7. Graphic user interface of control software

The length of the catheter tip part outside the guidewire was 40mm as shown in Fig. 4.8(a), with an initial tip direction along the z-axis. The driving currents were generated through a computer algorithm, especially developed to position the catheter tip within the central workspace. ProAnalyst® software was used to track the motion of the catheter tip from an initial position (zero electric currents) to a final equilibrium position (electric currents of 7A for all electromagnets), as shown in Fig. 4.8(b). Fig. 4.8(c) shows the progressive displacement of the catheter when the driving currents were gradually increased from 0A to 7A. ProAnalyst-based angle measurements showed an overall catheter tip bending angle of 52.71º (from the initial position to the final position), as shown in Fig. 4.8(b). The experimental results of the catheter movement displayed in Fig. 4.8 demonstrate the potential of the developed mathematical model as well as the principle of catheter tip positioning system.

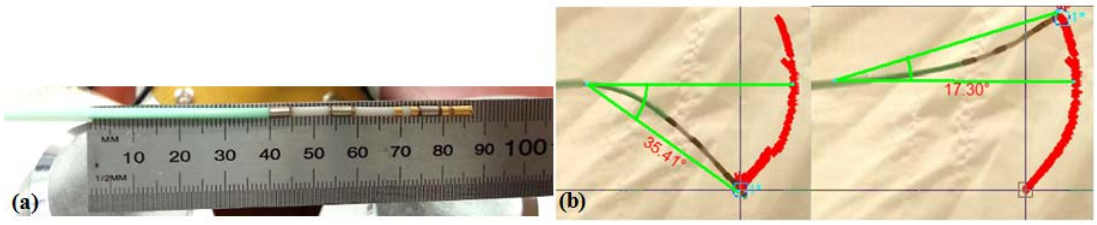

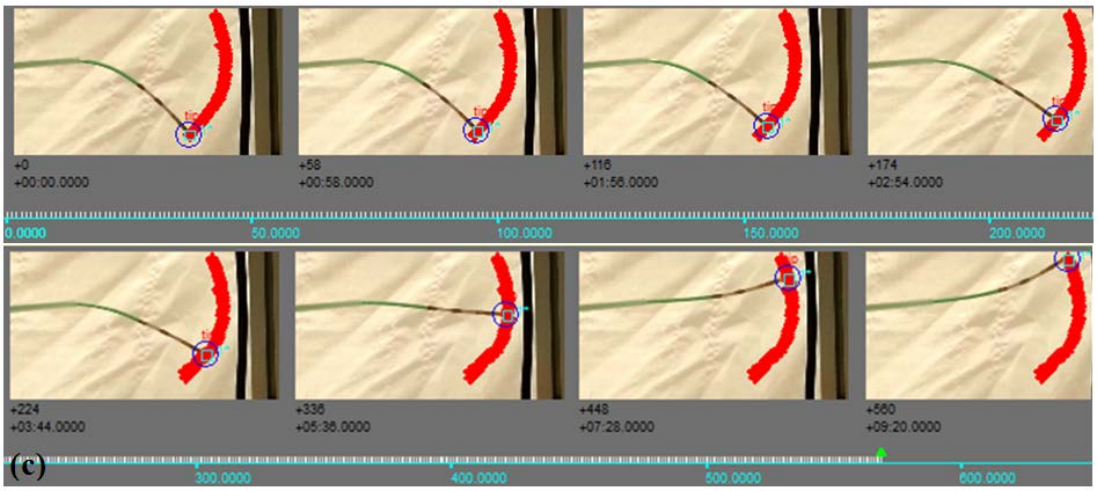

Fig. 4.8. (a) The 40-mm length of the catheter tip part outside the guidewire. (b) The catheter tip is bending up with the total angle 52.71º (35.41º +17.30 º) from the initial position to the final positon corresponding to the increment of electric currents. (c) Measured displacements and deflections of the catheter tip under an externally applied magnetic field with a set of electromagnet currents between 0A to 7A.

CHAPTER 5 CONCLUSION AND FUTURE WORK

5.1 Conclusions from this study

A comprehensive and accurate mathematical model has been developed, which accurately positions the deflection of a three-magnet tip catheter through an externally applied magnetic field. The magnetic field produced by the eight-electromagnet system has been accurately modelled. An analytical torque and force model takes into account the interaction between the three magnetic seeds attached to the catheter tip and the externally applied magnetic field. In addition, the developed iterative algorithm has been used, in conjunction with MATLAB's bvp4c solver, to predict the equilibrium condition of the catheter tip for arbitrary electromagnet current values. Finally, the ability of the developed mathematical model to predict the displacement, direction and deflection of the catheter tip as a function of the electromagnet current has been verified through experimental results.

5.2 Recommended future work

The mathematical model can be extended to calculate and predict the position of the catheter tip in a fluidic environment. There are more parameters related to the fluidic environment such as the viscosity of the blood, blood velocity and the damping force of the blood. This system also requires improvement to its speed to meet the demand for real-time control in the near future. More importantly, the bending angle of the catheter tip will need to be increased up to 180^{o} to push itself against cardiac tissue during ablation. It is desired to have a catheter that can bend up to 180^{o}. This will be addressed in the future. Typically, this function can be achieved by adjusting the torques and forces exerted on the three magnetic seeds of the catheter tip.

Appendix A & B has been excluded at the request of the author

REFERENCES

[1] R. Weerasooriya, P. Khairy, J. Litalien, L. Macle, M. Hocini, F. Sacher, *et al.*, "Catheter ablation for atrial fibrillation: are results maintained at 5 years of follow-up?," *Journal of the American College of Cardiology*, vol. 57, pp. 160-166, 2011.

[2] C. Bonanno, M. Paccanaro, L. La Vecchia, R. Ometto, and A. Fontanelli, "Efficacy and safety of catheter ablation versus antiarrhythmic drugs for atrial fibrillation: a meta-analysis of randomized trials," *Journal of Cardiovascular Medicine*, vol. 11, pp. 408-418, 2010.

[3] R. Cappato, H. Calkins, S.-A. Chen, W. Davies, Y. Iesaka, J. Kalman, *et al.*, "Updated worldwide survey on the methods, efficacy, and safety of catheter ablation for human atrial fibrillation," *Circulation: Arrhythmia and Electrophysiology*, vol. 3, pp. 32-38, 2010.

[4] O. Wazni, B. Wilkoff, and W. Saliba, "Catheter ablation for atrial fibrillation," *New England Journal of Medicine*, vol. 365, pp. 2296-2304, 2011.

[5] J. K.-R. Chun, S. Ernst, S. Matthews, B. Schmidt, D. Bansch, S. Boczor, *et al.*, "Remote-controlled catheter ablation of accessory pathways: results from the magnetic laboratory," *European heart journal*, vol. 28, pp. 190-195, 2007.

[6] H. Rafii-Tari, C. J. Payne, and G.-Z. Yang, "Current and Emerging Robot-Assisted Endovascular Catheterization Technologies: A Review," *Annals of biomedical engineering*, vol. 42, pp. 697-715, 2014.

[7] Y. Fu, H. Liu, W. Huang, S. Wang, and Z. Liang, "Steerable catheters in minimally invasive vascular surgery," *The International Journal of Medical Robotics and Computer Assisted Surgery*, vol. 5, pp. 381-391, 2009.

[8] J. Bradfield, R. Tung, R. Mandapati, N. G. Boyle, and K. Shivkumar, "Catheter ablation utilizing remote magnetic navigation: a review of applications and outcomes," *Pacing and Clinical Electrophysiology*, vol. 35, pp. 1021-1034, 2012.

[9] L. Flaction, "Intracorporeal anchoring and guiding system with permanent magnet force modulation," ÉCOLE POLYTECHNIQUE FÉDÉRALE DE LAUSANNE, 2013.

[10] E. S. Gang, B. L. Nguyen, Y. Shachar, L. Farkas, L. Farkas, B. Marx, *et al.*, "Dynamically Shaped Magnetic Fields Initial Animal Validation of a New Remote Electrophysiology Catheter Guidance and Control System," *Circulation: Arrhythmia and Electrophysiology*, vol. 4, pp. 770-777, 2011.

[11] M. P. Kummer, J. J. Abbott, B. E. Kratochvil, R. Borer, A. Sengul, and B. J. Nelson, "OctoMag: An Electromagnetic System for 5-DOF Wireless Micromanipulation," *IEEE Transactions on Robotics*, vol. 26, pp. 1006-1017, 2010.

[12] S. Erni, S. Schürle, A. Fakhraee, B. E. Kratochvil, and B. J. Nelson, "Comparison, optimization, and limitations of magnetic manipulation systems," *Journal of Micro-Bio Robotics*, vol. 8, pp. 107-120, 2013.

[13] Y. Shachar, "Apparatus and method for shaped magnetic field control for catheter, guidance, control, and imaging," ed: Google Patents, 2011.

[14] D. Filgueiras-Rama, A. Estrada, J. Shachar, S. Castrejón, D. Doiny, M. Ortega, *et al.*, "Remote Magnetic Navigation for Accurate, Real-time

Catheter Positioning and Ablation in Cardiac Electrophysiology Procedures," *Journal of visualized experiments: JoVE,* 2013.

[15] Y. Shachar, "Apparatus and method for shaped magnetic field control for catheter, guidance, control, and imaging," ed: Google Patents, 2012.

[16] W. a. N. Andrä, Hannes "Magnetism in medicine; a handbook, 2d ed," vol. 31, ed, 2007.

[17] H. Tillander, "Magnetic guidance of a catheter with articulated steel tip," *Acta Radiologica [Old Series],* vol. 35, pp. 62-64, 1951.

[18] H. Tillander, "Selective angiography with a catheter guided by a magnet," *Magnetics, IEEE Transactions on,* vol. 6, pp. 355-358, 1970.

[19] I. Tunay, "Modeling magnetic catheters in external fields," *Conference proceedings : ... Annual International Conference of the IEEE Engineering in Medicine and Biology Society. IEEE Engineering in Medicine and Biology Society. Conference,* vol. 3, p. 2006, 2004.

[20] G. Gillies, R. Ritter, W. Broaddus, M. Grady, M. Howard III, and R. McNeil, "Magnetic manipulation instrumentation for medical physics research," *Review of Scientific Instruments,* vol. 65, pp. 533-562, 1994.

[21] H. Keller, A. Juloski, H. Kawano, M. Bechtold, A. Kimura, H. Takizawa, *et al.*, "Method for navigation and control of a magnetically guided capsule endoscope in the human stomach," in *Biomedical Robotics and Biomechatronics (BioRob), 2012 4th IEEE RAS & EMBS International Conference on*, 2012, pp. 859-865.

[22] D. B. Camarillo, T. M. Krummel, and J. K. Salisbury Jr, "Robotic technology in surgery: past, present, and future," *The American Journal of Surgery,* vol. 188, pp. 2-15, 2004.

[23] R. D. Brewer, K. E. Loewke, E. F. Duval, and J. K. Salisbury, "Force control of a permanent magnet for minimally-invasive procedures," in *Biomedical Robotics and Biomechatronics, 2008. BioRob 2008. 2nd IEEE RAS & EMBS International Conference on*, 2008, pp. 580-586.

[24] R. C. Diggery and D. T. Grint, *Catheters: Types, Applications and Potential Complications*: Nova Science Publishers, Incorporated, 2011.

[25] J. Driller, "Kinetics of magnetically guided catheters," *Magnetics, IEEE Transactions on,* vol. 6, pp. 467-471, 1970.

[26] M. N. Faddis, W. Blume, J. Finney, A. Hall, J. Rauch, J. Sell, *et al.*, "Novel, magnetically guided catheter for endocardial mapping and radiofrequency catheter ablation," *Circulation,* vol. 106, pp. 2980-2985, 2002.

[27] O. Ergeneman, C. Bergeles, M. P. Kummer, J. J. Abbott, and B. J. Nelson, "Wireless intraocular microrobots: Opportunities and challenges," in *Surgical Robotics*, ed: Springer, 2011, pp. 271-311.

[28] J. J. Abbott, O. Ergeneman, M. P. Kummer, A. M. Hirt, and B. J. Nelson, "Modeling magnetic torque and force for controlled manipulation of soft-magnetic bodies," *Robotics, IEEE Transactions on,* vol. 23, pp. 1247-1252, 2007.

[29] Magnetecs. (2011). *Magnetecs CGCI Receives CE Marking for Sales in Europe*. Available: http://magnetecs.com/news.php?id=67

[30] S. Ernst, F. Ouyang, C. Linder, K. Hertting, F. Stahl, J. Chun, *et al.*, "Initial experience with remote catheter ablation using a novel magnetic navigation system magnetic remote catheter ablation," *Circulation,* vol. 109, pp. 1472-1475, 2004.

[31] F. Carpi and C. Pappone, "Stereotaxis Niobe® magnetic navigation system for endocardial catheter ablation and gastrointestinal capsule endoscopy," *Expert Review of Medical Devices,* vol. 6, pp. 487-498, 2009.
[32] Y. Ganji and F. Janabi-Sharifi, "Catheter kinematics for intracardiac navigation," *Biomedical Engineering, IEEE Transactions on,* vol. 56, pp. 621-632, 2009.
[33] M. N. Faddis and B. D. Lindsay, "Magnetic catheter manipulation," *Coronary artery disease,* vol. 14, pp. 25-27, 2003.
[34] J. Cadeddu, R. Fernandez, M. Desai, R. Bergs, C. Tracy, S.-J. Tang, *et al.*, "Novel magnetically guided intra-abdominal camera to facilitate laparoendoscopic single-site surgery: initial human experience," *Surgical endoscopy,* vol. 23, pp. 1894-1899, 2009.
[35] T. Krings, J. Finney, P. Niggemann, P. Reinacher, N. Lück, A. Drexler, *et al.*, "Magnetic versus manual guidewire manipulation in neuroradiology: in vitro results," *Neuroradiology,* vol. 48, pp. 394-401, 2006.
[36] T. Szili-Torok and F. Akca, "Remote magnetic navigation in atrial fibrillation," 2012.
[37] A. Da Costa, M. Ben H'Dech, C. Romeyer-Bouchard, L. Bisch, A. Gate-Martinet, M. Levallois, *et al.*, "Remote-controlled magnetic pulmonary vein isolation using a new three-dimensional non-fluoroscopic navigation system: A single-centre prospective study," *Archives of cardiovascular diseases,* vol. 106, pp. 423-432, 2013.
[38] A. S. Thornton and L. J. Jordaens, "Remote magnetic navigation for mapping and ablating right ventricular outflow tract tachycardia," *Heart Rhythm,* vol. 3, pp. 691-696, 2006.
[39] M. S. PATTERSON, J. SCHOTTEN, C. VAN MIEGHEM, F. KIEMENEIJ, and P. W. SERRUYS, "Magnetic navigation in percutaneous coronary intervention," *Journal of interventional cardiology,* vol. 19, pp. 558-565, 2006.
[40] Stereotaxis. Available: www.stereotaxis.com
[41] K. Halbach, "Design of permanent multipole magnets with oriented rare earth cobalt material," *Nuclear instruments and methods,* vol. 169, pp. 1-10, 1980.
[42] F. Creighton, "Optimal distribution of magnetic material for catheter and guidewire cardiology therapies," in *Magnetics Conference, 2006. INTERMAG 2006. IEEE International*, 2006, pp. 111-111.
[43] Z. Issa, J. M. Miller, and D. P. Zipes, *Clinical Arrhythmology and Electrophysiology: A Companion to Braunwald's Heart Disease: Expert Consult: Online and Print*: Elsevier Health Sciences, 2012.
[44] S. Ramcharitar, M. S. Patterson, R. J. van Geuns, C. van Meighem, and P. W. Serruys, "Technology insight: magnetic navigation in coronary interventions," *Nature Clinical Practice Cardiovascular Medicine,* vol. 5, pp. 148-156, 2008.
[45] B. L. Nguyen, J. L. Merino, and E. S. Gang, "Remote Navigation for Ablation Procedures â A New Step Forward in the Treatment of Cardiac Arrhythmias," 2010.
[46] M. P. Armacost, J. Adair, T. Munger, R. R. Viswanathan, F. M. Creighton, D. T. Curd, *et al.*, "Accurate and reproducible target navigation with the stereotaxis Niobe® magnetic navigation system," *Journal of Cardiovascular Electrophysiology,* vol. 18, pp. S26-S31, 2007.

[47] B. Schmidt, K. R. J. Chun, R. R. Tilz, B. Koektuerk, F. Ouyang, and K.-H. Kuck, "Remote navigation systems in electrophysiology," *Europace*, vol. 10, pp. iii57-iii61, 2008.
[48] A. Scientific. (2010). *Aeon Phocus*. Available: http://www.aeon-scientific.com/
[49] I. B. Ray, S. Dukkipati, C. Houghtaling, C. D. McPherson, N. Kastelein, J. N. Ruskin, *et al.*, "Initial Experience with a Novel Remote-Guided Magnetic Catheter Navigation System for Left Ventricular Scar Mapping and Ablation in a Porcine Model of Healed Myocardial Infarction," *Journal of cardiovascular electrophysiology*, vol. 18, pp. 520-525, 2007.
[50] J. Svoboda, *Magnetic techniques for the treatment of materials* vol. 641: Springer, 2004.
[51] M. Poole, P. Weiss, H. S. Lopez, M. Ng, and S. Crozier, "Minimax current density coil design," *Journal of Physics D: Applied Physics*, vol. 43, p. 095001, 2010.
[52] R. A. Serway, J. W. Jewett, K. Wilson, and A. Wilson, *Physics*. South Melbourne, Vic: Cengage Learning Australia, 2013.
[53] L. Muller, M. Saeed, M. W. Wilson, and S. W. Hetts, "Remote control catheter navigation: options for guidance under MRI," *J Cardiovasc Magn Reson*, vol. 14, p. 33, 2012.
[54] H. Abbott RealTime, "SUMMARY OF SAFETY AND EFFECTIVENESS DATA (SSED)."
[55] P. Peichl and J. Kautzner, "Advances in irrigated tip catheter technology for treatment of cardiac arrhythmias," *Recent patents on cardiovascular drug discovery*, vol. 8, pp. 10-16, 2013.
[56] S. Ernst, "Magnetic Navigation: Description of Technique, Advantages, and Technical Issues," in *Cardiac Imaging in Electrophysiology*, A. Auricchio, J. Singh, and F. E. Rademakers, Eds., ed: Springer London, 2012, pp. 299-303.
[57] B. Muntean, K.-J. Gutleben, J. Heintze, J. Vogt, D. Horstkotte, and G. Nölker, "Magnetically guided irrigated gold-tip catheter ablation of persistent atrial fibrillation—techniques, procedural parameters and outcome," *Journal of interventional cardiac electrophysiology*, vol. 35, pp. 163-171, 2012.
[58] D.-I. Shin and T. Deneke, "Ablation catheters for atrial fibrillation: benefits and complications," *Therapy*, vol. 7, pp. 133-138, 2010.
[59] Z. Nagy, O. Ergeneman, J. J. Abbott, M. Hutter, A. M. Hirt, and B. J. Nelson, "Modeling assembled-MEMS microrobots for wireless magnetic control," in *Robotics and Automation, 2008. ICRA 2008. IEEE International Conference on*, 2008, pp. 874-879.
[60] D. C. Jiles, *Introduction to magnetism and magnetic materials*: CRC Press, 1998.
[61] F. P. Gosselin, V. Lalande, and S. Martel, "Characterization of the deflections of a catheter steered using a magnetic resonance imaging system," *Medical physics*, vol. 38, pp. 4994-5002, 2011.
[62] F. Settecase, M. S. Sussman, M. W. Wilson, S. Hetts, R. L. Arenson, V. Malba, *et al.*, "Magnetically-assisted remote control (MARC) steering of endovascular catheters for interventional MRI: a model for deflection and design implications," *Medical physics*, vol. 34, pp. 3135-3142, 2007.
[63] I. S. Grant and W. R. Phillips, *Electromagnetism*. Hoboken: Wiley, 2013.
[64] S. Floyd, C. Pawashe, and M. Sitti, "An untethered magnetically actuated micro-robot capable of motion on arbitrary surfaces," in *Robotics and*

Automation, 2008. ICRA 2008. IEEE International Conference on, 2008, pp. 419-424.

[65] T. H. Boyer, "The force on a magnetic dipole," *Am. J. Phys*, vol. 56, pp. 688-692, 1988.

[66] H. Marino, C. Bergeles, and B. J. Nelson, "Robust $\mathcal{H}\infty$ control for electromagnetic steering of microrobots," in *Robotics and Automation (ICRA), 2012 IEEE International Conference on*, 2012, pp. 2498-2503.

[67] E. J. Hearn and Ebrary, *Mechanics of Materials: Vol. 1: An Introduction to the Mechanics of Elastic and Plastic Deformation of Solids and Structural Materials*. San Diego: Butterworth-Heinemann [Imprint], 1997.

[68] R. P. Feynman, R. B. Leighton, and M. Sands, "Feynman Lectures on Physics, Vol. II–The New Millennium Edition: Mainly Electromagnetism and Matter," ed: Basic Books (New York), 2011.

[69] A. Kimiaeifar, N. Tolou, A. Barari, and J. Herder, "Large deflection analysis of cantilever beam under end point and distributed loads," *Journal of the Chinese Institute of Engineers*, vol. 37, pp. 438-445, 2014.

[70] T. Beléndez, C. Neipp, and A. Beléndez, "Large and small deflections of a cantilever beam," *European Journal of Physics*, vol. 23, p. 371, 2002.

[71] S. S. Bhavikatti, Ebrary, and I. ebrary, *Mechanics of solids*. New Delhi: New Age International, 2010.

[72] M. Scaglione, L. Biasco, D. Caponi, M. Anselmino, A. Negro, P. Di Donna, *et al.*, "Visualization of multiple catheters with electroanatomical mapping reduces X-ray exposure during atrial fibrillation ablation," *Europace*, vol. 13, pp. 955-962, 2011.

[73] J. Jin, *The finite element method in electromagnetics*: John Wiley & Sons, 2014.

[74] G. Apaydin, "Efficient finite-element method for electromagnetics," *Antennas and Propagation Magazine, IEEE*, vol. 51, pp. 61-71, 2009.

[75] M. V. K. Chari and S. J. Salon, *Numerical methods in electromagnetism*. US: Academic Press, 2000.

[76] M. N. Sadiku, *Numerical techniques in electromagnetics*: CRC press, 2000.

[77] H. Marino, C. Bergeles, and B. J. Nelson, "Robust Electromagnetic Control of Microrobots Under Force and Localization Uncertainties," *IEEE Transactions on Automation Science and Engineering*, vol. 11, pp. 310-316, 2014.

[78] M. W. Spong and M. Vidyasagar, *Robot dynamics and control*: John Wiley & Sons, 2008.

[79] D. D. VILLANI, "An analytic solution for the force between two magnetic dipoles," *Magnetic and Electrical Separation*, vol. 9, pp. 39-52, 1998.

[80] G. Nölker, K.-J. Gutleben, B. Muntean, J. Vogt, D. Horstkotte, L. D. Abkenari, *et al.*, "Novel robotic catheter manipulation system integrated with remote magnetic navigation for fully remote ablation of atrial tachyarrhythmias: a two-centre evaluation," *Europace*, p. eus169, 2012.

[81] K. B. Yesin, K. Vollmers, and B. J. Nelson, "Modeling and control of untethered biomicrorobots in a fluidic environment using electromagnetic fields," *The International Journal of Robotics Research*, vol. 25, pp. 527-536, 2006.

[82] J. Kauphusman, H. Wang, J. Dando, and H. Puryear, "Irrigated ablation catheter having magnetic tip for magnetic field control and guidance," ed: Google Patents, 2007.

[83] T. T. Tegg and J. V. Kauphusman, "Magnetically guided catheters," ed: Google Patents, 2010.
[84] A. de la Rama, C. Pappone, P. C. Chen, C. Hata, and J. A. Shimizu, "Magnetically guided catheter with flexible tip," ed: Google Patents, 2014.
[85] A. Banerjee, B. Bhattacharya, and A. Mallik, "Large deflection of cantilever beams with geometric non-linearity: Analytical and numerical approaches," *International Journal of Non-Linear Mechanics,* vol. 43, pp. 366-376, 2008.
[86] T. Wang, S. Lee, and O. Zienkiewicz, "A numerical analysis of large deflections of beams," *International Journal of Mechanical Sciences,* vol. 3, pp. 219-228, 1961.
[87] L. F. Shampine, J. Kierzenka, and M. W. Reichelt, "Solving boundary value problems for ordinary differential equations in MATLAB with bvp4c," *Tutorial notes,* 2000.
[88] J. Kierzenka and L. F. Shampine, "A BVP solver based on residual control and the Maltab PSE," *ACM Transactions on Mathematical Software (TOMS),* vol. 27, pp. 299-316, 2001.
[89] L. Shampine, "Solving a hard BVP with bvp4c," *private communication,* 2004.